J Neurophysiol 108: 2033–2050, 2012.
First published July 18, 2012; doi:10.1152/jn.00936.2011.

Effects of contrast and contrast adaptation on static receptive field features in macaque area V1

Jean-Baptiste Durand, Pascal Girard, Pascal Barone, Jean Bullier, and Lionel G. Nowak
Centre de Recherche Cerveau et Cognition, Université Toulouse 3-CNRS, Toulouse, France

Submitted 17 October 2011; accepted in final form 11 July 2012

Durand JB, Girard P, Barone P, Bullier J, Nowak LG. Effects of contrast and contrast adaptation on static receptive field features in macaque area V1. *J Neurophysiol* 108: 2033–2050, 2012. First published July 18, 2012; doi:10.1152/jn.00936.2011.—The spatiotemporal features of the "static" receptive field (RF), as revealed with flashing bars or spots, determine other RF properties. We examined how some of these static RF features vary with contrast and contrast adaptation in area V1 of the anesthetized macaque monkey. RFs were mapped with light and dark flashing bars presented at three different contrasts, with the low and medium contrasts eliciting approximately 1/3 and 2/3 of the high-contrast response amplitude. The main results are as follows: *1*) RF widths decreased when contrast decreased; however, the amount of decrease was less than that expected from an iceberg model and closer to the expectation of a contrast invariance of the RF width. *2*) Area tuning experiments with drifting gratings showed an opposite effect of contrast: an increase in preferred stimulus diameter when contrast decreased. This implies that the effect of contrast on preferred stimulus size is not predictable from the static RF. *3*) Contrast adaptation attenuated the effect of contrast on RF amplitude but did not significantly modify RF width. *4*) RF subregion overlap was only marginally affected by changes in contrast and contrast adaptation; the classification of cells as simple and complex, when established from subregion overlap, appears to be robust with respect to changes in contrast and adaptation state. Previous studies have shown that the spatiotemporal features of the RF depend largely on the stimuli used to map the RF. This study shows that contrast is one elemental feature that contributes to the dynamics of the RF.

adaptation; contrast; static receptive field; V1; vision

THE RECEPTIVE FIELDS (RFs) of primary visual cortex neurons have been extensively characterized with static flashing bars or spots (DeAngelis et al. 1993a; Heggelund 1981; Jones and Palmer 1987a; Movshon et al. 1978a, 1978b; Palmer and Davis 1981; Rust et al. 2005). We refer to the RFs revealed with such static stimuli as the "static RFs." Two broad classes of static RFs have been identified: simple RFs, characterized by "on" and "off" subregions that show little spatial overlap, and complex RFs, characterized by "on" and "off" subregions that overlap strongly in both space and time (see, e.g., Hubel and Wiesel 1962; Schiller et al. 1976).

In simple cells, the static RF contains the seeds for other RF properties. For instance, the optimal orientation of the RF is determined by the shape and spatial organization of the constituent subregions (Gardner et al. 1999; Heggelund and Moors 1983; Jones and Palmer 1987b; Niell and Stryker 2008; Sharpee et al. 2008; Usrey et al. 2003), while the optimal spatial frequency can be predicted from the number and width of the subregions (DeAngelis et al. 1993b; Field and Tolhurst 1986; Jones and Palmer 1987b; Movshon et al. 1978a; Smyth et al. 2003). In complex cells, the static RF is composed of subunits, which show spatiotemporal features resembling simple RFs (Baker and Cynader 1986; Chen et al. 2007; Conway and Livingstone 2003; Emerson et al. 1987; Movshon et al. 1978b; Pack et al. 2006; Rust et al. 2005; Sasaki and Ohzawa 2007; Szulborski and Palmer 1990; Touryan et al. 2005). Stimulus preference in complex cells might also be specified by the spatiotemporal organization of these subunits (Chen et al. 2007; Movshon et al. 1978b; Rust et al. 2005; Szulborski and Palmer 1990; Touryan et al. 2005).

In addition to the optimal stimuli, the tuning for orientation and spatial frequency can also be predicted from the spatiotemporal organization of the static RF (Andrews and Pollen 1979; DeAngelis et al. 1993b; Field and Tolhurst 1986; Gardner et al. 1999; Heggelund and Moors 1983; Movshon et al. 1978a, 1978b; Touryan et al. 2005; Usrey et al. 2003). The prediction quality is often fairly good, but it may be improved by examining the synaptic RF (Lampl et al. 2001; Nowak et al. 2010) and by taking input-output nonlinearities into account (Albrecht and Geisler 1991; DeAngelis et al. 1993b; Gardner et al. 1999; Priebe and Ferster 2005; Reid et al. 1991).

Studies have shown that in rodents and carnivores the tuning for orientation and spatial frequency, when assessed with drifting bars or gratings, does not change when the contrast is modified (Albrecht and Hamilton 1982; Alitto and Usrey 2004; Anderson et al. 2000; Carandini and Sengpiel 2004; Finn et al. 2007; Li and Creutzfeldt 1984; Niell and Stryker 2008; Sclar and Freeman 1982; Skottun et al. 1987; Van Hooser et al. 2005). If the static RF is the seed for these contrast-invariant RF properties, then one would expect that the spatiotemporal features of the static RF are also contrast-invariant. Whether the static RF is indeed contrast-invariant constitutes one of the main questions of the present investigation.

However, other RF properties predict that the static RF features should not be contrast-invariant. In particular, size-tuning experiments using drifting gratings consistently showed that the apparent preferred stimulus size increases when stimulus contrast decreases (Cavanaugh et al. 2002; Kapadia et al. 1999; Sceniak et al. 1999; Sengpiel et al. 1997; Shushruth et al. 2009; Song and Li 2008; Tailby et al. 2007). This expansion at low contrast potentially results from an expansion of the static RF (Kapadia et al. 1999; Sceniak et al. 1999)—hence, lack of contrast invariance (but see Cavanaugh et al. 2002; Song and Li 2008). Sceniak et al. (2002) also showed that the spatial frequency tuning in primates is not contrast-invariant, and this further substantiates the possibility of an expansion of the static RF at low contrast.

Address for reprint requests and other correspondence: L. G. Nowak, Centre de Recherche Cerveau et Cognition, Université Toulouse 3-CNRS, Toulouse, France (e-mail: lionel.nowak@cerco.ups-tlse.fr).

Another issue examined in this study was the susceptibility of static RF features to contrast adaptation. Contrast adaptation refers here to the slow adjustment of the firing rate that is observed during prolonged exposure to a stimulus of constant contrast (see, e.g., Albrecht et al. 1984; Maffei et al. 1973; Sanchez-Vives et al. 2000; Sclar et al. 1989). We recently showed that, in primate area V1, contrast adaptation does contribute to contrast invariance of orientation tuning (Nowak and Barone 2009). Size tuning also has been shown to vary depending on the adaptation state of the neurons (Cavanaugh et al. 2002). Altogether, these results suggest that the static RF features may also depend on the adaptation state of the neurons under study.

Another property that may not show contrast invariance is the linearity of spatial summation. This linearity is typically characterized by the "relative modulation" (RM), the ratio of the first harmonic to the mean of the Fourier transform of the responses to sine-wave drifting gratings (Skottun et al. 1991). The RM allows partitioning between linear, simplelike RFs (RM $>$ 1) and nonlinear, complexlike RFs (RM $<$ 1). In simple cells, RM does not vary much with contrast (Tolhurst and Dean 1990), but a recent study (Crowder et al. 2007) showed that complex cells become more simplelike when the contrast is decreased. The same study also reported that RM and related simple/complex cell partitioning are affected by contrast adaptation. These results predict that, in the static RF of complex cells, subregions should overlap less after adaptation or when the contrast is lowered.

To determine whether they are contrast-invariant, we mapped the static RFs of neurons in area V1 of the macaque, using light and dark bars presented at three different contrasts. We found that the width of the static RF was reduced when the contrast was decreased. This effect of contrast was opposite to that observed on preferred stimulus diameter determined from size-tuning measurements in the same cells. Finally, we found that the RF categories, as identified by high-frequency flashing stimuli, remain steady with respect to changes in contrast and contrast adaptation.

Altogether, our results provide further evidence that the spatiotemporal features of the RFs largely depend on the stimulus features—here the contrast and its temporal variance. A strong implication of these results is that the static RF does not allow prediction of all RF tuning properties and their contrast dependence, and that both functional connectivity and nonlinearities need to be taken into account.

METHODS

Surgical Protocol

The surgical procedures were similar to those described in previous publications (Girard et al. 1992; Nowak et al. 1995). Experiments were performed on three male cynomolgus macaques (*Macaca fascicularis*) weighting 8–10 kg. Anesthesia was induced with ketamine hydrochloride (16 mg/kg). Atropine (0.05 mg/kg) was injected subcutaneously to reduce secretions and to prevent bradycardia. The saphenous or the ulnar vein was catheterized, and anesthesia was maintained throughout the surgery by intravenous Alphadalone/Alphaxalone acetate (Saffan, Essex Pharma) injection (0.25–0.5 ml every 10–15 min). Synthetic corticoid, Dexamethasone (Merck) or Solu-Medrol (Pfizer), was given to prevent brain edema (1 mg/kg im). The animal's body temperature was maintained at 37°C with a heating pad controlled by a rectal thermistor (Harvard Apparatus). The ECG was continuously monitored. Blood pressure was recorded through an arterial catheter inserted in the femoral artery. A tracheotomy was performed, and a tracheal tube was inserted to allow artificial ventilation. The monkey was then set in a stereotaxic frame. Holes were drilled over the frontal cortex to allow for epidural EEG recording, and a craniotomy was made to gain access to area V1. A head post was sealed with screws and dental acrylic to the skull and fixed to the stereotaxic apparatus. Ear, eye, and mouth bars were then removed. All incision sites were infiltrated with lidocaine.

After surgery and during recording, the animal was artificially ventilated with N_2O-O_2 (70%-30%). Anesthesia and analgesia were supplemented by a continuous infusion of sufentanil citrate (Sufenta, Janssen; 4–6 $\mu g \cdot kg^{-1} \cdot h^{-1}$) in 5% glucose solution, after a loading dose of 1 μg/kg. Paralysis was maintained by continuous injection of pancuronium bromide (Pavulon, Organon, 0.076 $\mu g \cdot kg^{-1} \cdot h^{-1}$) in lactated Ringer solution + glucose 5%, after a loading dose of 0.1 mg/kg. Broadband antibiotics were injected (im) every day.

Mydriasis and cycloplegia were induced with ophthalmic atropine sulfate (1%, Alcon). Neutral contact lenses were used to protect the eyes. The lenses were cleaned every day, and neomycin sulfate (0.25 mg/ml, Sanofi-Aventis) eye drops were applied to prevent infection. Optic disks were located with a reversible ophthalmoscope. Correcting lenses were added to focus the eyes on a screen placed at 114 cm.

Heart rate, EEG, blood pressure, and end-tidal CO_2 were continuously monitored to ensure a proper degree of analgesia. This protocol was in accordance with the guidelines from the European Community (directive 86/609) and from the French Ministry of Agriculture (décret 87/848) and was approved by the local ethical committee (MP/02/02/01/05, Comité régional d'éthique pour l'expérimentation animale, Midi-Pyrénées).

Recording Procedure and Spike Sorting

Action potentials were recorded extracellularly through tungsten-in-glass microelectrodes (Merrill and Ainsworth 1972). After amplification and band-pass filtering, action potentials were acquired with a Power1401 interface and Spike2 software (CED, Cambridge, UK) with a digitization rate of 40–50 kHz. The collected signal usually contained spikes from multiple units. Spike sorting was performed off-line with the algorithm of Fee et al. (1996) implemented in MATLAB. Spikes were considered to be issued from one single neuron if the interspike interval histogram demonstrated an absolute refractory period $>$1 ms.

Visual Stimulation

The approximate location of the RF was first determined with a handheld projector. Eye preference was then determined, and all subsequent visual stimuli were delivered through the dominant eye. Computer-controlled stimuli were generated with a VSG2/2F board (CRS, Cambridge, UK) and were presented on a Daewoo CMC-2100 ME 21-in. color monitor (100 Hz noninterlaced refresh, 640 $\times$ 487 resolution) in the first two experiments. In the third experiment, stimuli were generated with a VSG Visage system and were presented on a 22-in. Mitsubishi Diamond Pro 2070^{SB} color monitor (100 Hz noninterlaced refresh, 800 $\times$ 600 resolution). Proper luminance and contrast production were ensured after gamma correction. The contrast corresponds to Michelson's contrast, defined relative to the maximal and minimal luminance (L_{max} and L_{min}, respectively) of the gratings and bars as $C(\%) = 100 \times (L_{max} - L_{min})/(L_{max} + L_{min})$. The background luminance was 14 cd/m^2 in the first two experiments and 30 cd/m^2 in the last experiment.

Optimal stimuli were quantitatively evaluated from peristimulus time histograms (PSTHs) calculated online. The preferred orientation and preferred spatial frequency of the cells or cell clusters and the contrast-response function were determined as previously described (Nowak and Barone 2009). For refining the estimate of RF location,

square-wave gratings were presented within a square window of 1° width in a grid of 4 × 4 positions. From the contrast-response function, three contrast values were extracted: one causing ~80–90% of the maximal response ("high contrast"), one causing 20–25% of the maximal response ("low contrast"), and one causing ~50% of the maximal response ("medium contrast").

Quantitative analysis of the static RFs relied on a forward correlation method. The stimulation paradigm consisted of flashing a single bar that was either darker or brighter than the background ("sparse noise"; adapted from DeAngelis et al. 1993a; Jones and Palmer 1987a). For each presentation, the bar occupied 1 randomly chosen position among 16 available. The bar presentation lasted 50 ms in some recordings and 100 ms in the others. The orientation of the bar corresponded to the orientation that was optimal for the recording site,[1] and the bar positions varied along the axis perpendicular to this orientation. The mapping was restricted to this single dimension. The bar width was initially chosen to be one-fifth of the spatial period corresponding to the cell's preferred spatial frequency and was further adjusted by running preliminary tests checking the cell's response as a function of the bar positions. Centering of the stimulus array was also checked and modified if required. Adjacent positions were spaced apart by a distance equal to the bar width. The bar width was 0.25 ± 0.17° (mean ± SD; range: 0.05–0.80°). The bar length was 7–30 times the bar width (mean ± SD: 16.46 ± 4.91). The stimulated area represented 4.08 ± 2.80° of visual angle (range: 0.80–12.80°).

Three pairs of light and dark luminance values were used, with small, intermediate, and large departures relative to the background luminance (see Fig. 2*A*). The mean luminance for each pair was equal to the background luminance. The three pairs of luminance values define the three contrast levels used for mapping the RF. Bar contrast was initially set to the low, medium, and high values determined from the contrast-response function. However, only a few cells displayed significant responses with the flashing bars at the lowest contrast thus defined, possibly as a consequence of a difference in stimulus energy between the (small) flashing bars and the (larger) drifting gratings used to establish the contrast-response function, and also possibly because of differences in gain control for flashing versus drifting stimuli (Cardin et al. 2008). Therefore, in subsequent experiments the response to the bars at low and medium contrasts was checked by running preliminary RF mappings, and the contrasts were increased if necessary. On average, the low and medium contrasts finally chosen elicited approximately one-third and two-thirds of the response at high contrast (see Fig. 4).

Our first aim was to determine whether, and how, contrast modified the features of the static RF. Our second aim was to determine the consequences of contrast adaptation on these features. We adapted the protocol of Nowak and Barone (2009) to fulfill these aims; it is depicted in Fig. 2*A*. In the first block of stimulus presentation (Fig. 2*A*, *left*, "mixed contrasts"), the contrast of the bar could take, randomly, one of the three preset values (low, medium, and high). Thus in this first block, which lasted 34–82 s, both bar position and contrast varied randomly every 50 or 100 ms. The randomization protocol was "blockwise," with no repeats of a given stimulus until all 96 individual stimuli (2 polarities × 3 contrasts × 16 positions) have been presented. Contrast adaptation being a relatively slow phenomenon (>100 ms; Albrecht et al. 1984; McLean and Palmer 1996; Müller et al. 1999; Nelson 1991; Nowak and Barone 2009; Ohzawa et al. 1985; Sanchez-Vives et al. 2000; Sclar et al. 1989), it could not occur for each contrast during this first block. However, adaptation possibly occurred for a contrast value representing the mean of the three contrasts in use. The slow time course of contrast adaptation therefore led to a mismatch between the contrast presented at one particular moment and the contrast to which the cell was adapted.

In the second, third, and fourth stimulus presentation blocks, the contrast within each block was fixed: in the second block to the low contrast only, in the third block to the medium contrast only, and in the fourth block to the high contrast only. These blocks correspond to the "constant-contrast" conditions (Fig. 2*A*, *right*). Each block lasted 16–30 s, such that neurons had enough time to adapt to the unique contrast used in each block. The contrast presented at any time and the adapting contrast did match in this condition.

The four stimulation blocks were separated by blank periods lasting 5 s with only the background present. The complete stimulation sequence (mixed + constant contrast blocks) was repeated at least 10 times.

In the third monkey, we also performed size-tuning experiments using sinusoidal drifting gratings. This allowed comparison of the effect of contrast on the preferred grating size with those on the static RF size in the same cells. The three contrast values used for the RF mapping were also used for the size-tuning experiments. Nine different diameters were presented, from 0.20° up to 9.70° in power of 2 steps ($2^{0.7}$). Each stimulus was presented for 3 s. Both contrasts and diameters were randomly interleaved.

Histology and Electrode Tract Reconstruction

After completion of an electrode track, two or three electrolytic lesions (10 mA, 10 s) were made at different depths through the recording microelectrode. The animals were killed with a lethal intravenous injection of pentobarbital sodium. They were perfused transcardially with 0.9% saline followed by 4% paraformaldehyde in phosphate buffer. Cryoprotection was insured by overnight immersion in 30% sucrose solution. Parasagittal sections, 40 μm thick, were cut on a freezing microtome. Cortical layers were revealed with cresyl violet stain. Recording site positions were reconstructed relative to the electrolytic lesion positions.

Data Analysis

All analyzes were performed off-line after single-unit isolation.

Adaptation during presentation of constant contrast. The presence or lack of significant firing rate adaptation during the presentation of high-, medium-, or low-contrast stimuli was determined by Abeles' method (1982), based on confidence intervals calculated on spike counts. For this purpose, we calculated a PSTH for each contrast with a bin width of 4 s, with *time 0* corresponding to the beginning of a block. The number of spikes in the first bin, x, was used to calculate the 95% confidence limits, $L_{95\%}$:

$$L_{95\%} = x \pm 2.583 \times \sqrt{x}$$

Adaptation was considered significant when the spike count in the fourth bin (12–16 s) was less than the lower 95% confidence limit. Neurons were considered "nonadapting" if the number of spikes in the fourth bin was within the confidence interval. The proportion of neurons demonstrating a significant adaptation is represented in Fig. 1*A*. This proportion decreased when contrast decreased, from 50% with high-contrast stimuli, to 24% with medium-contrast stimuli, to 11% with low-contrast stimuli.

Time course of adaptation. The time constant of adaptation, τ, was determined in the cells that showed a significant adaptation. PSTHs were calculated for each contrast with a bin width of 1 s. The firing rate decay was fit with a single exponential. Time constants were not considered if the r^2 of fit was <0.6. Figure 1*B* presents one example. The adaptation time constants were 0.65 s and 0.50 s for the high and medium contrasts, respectively. At the population level (Fig. 1*C*), the median time constants were 1.55 (n = 34), 1.93 (n = 8), and 2.39 (n = 1) s for high, medium, and low contrasts, respectively. This is considerably less than the values reported when the stimulus is a

[1] The online assessment of preferred orientation was based on multiunit recording. After off-line spike sorting, it sometimes happened that the preferred orientation of the isolated single units differed from that of the multiunit. Differences were relatively minor, however, in the majority of cases (<30° for 85% of the single units).

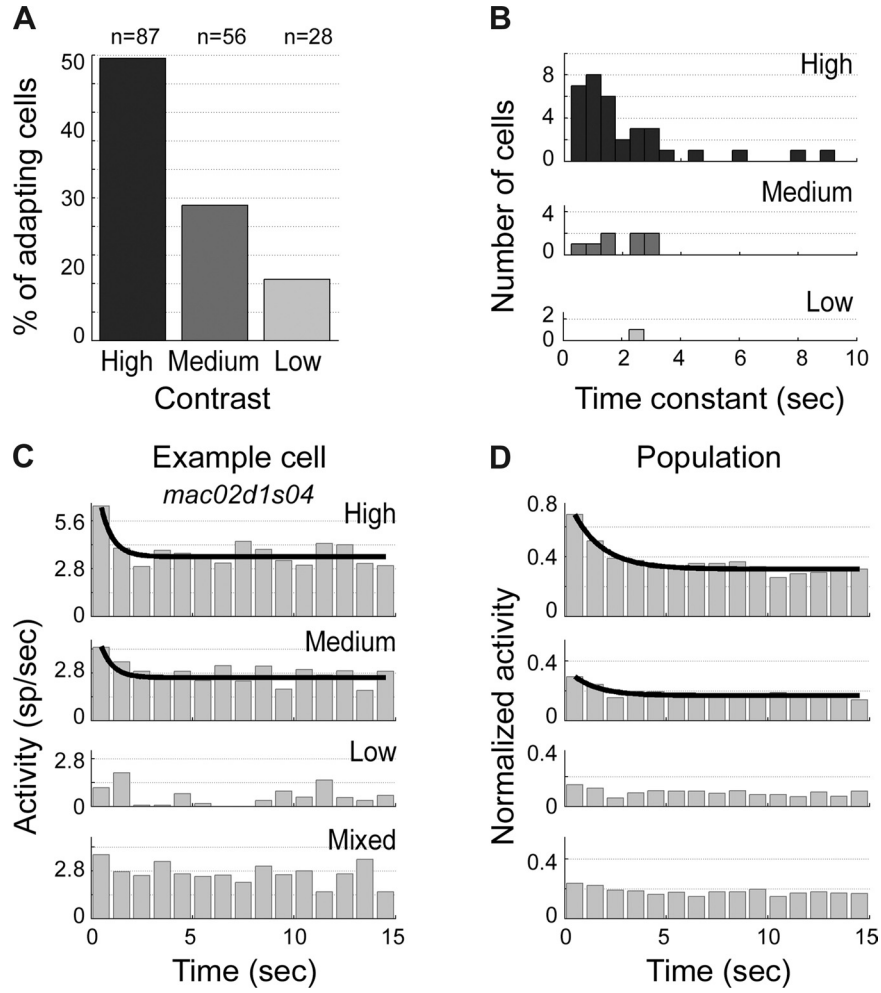

Fig. 1. Incidence and time constant of adaptation. *A*: proportion of cells showing a significant adaptation during constant-contrast stimulation blocks. *B*: distribution of the time constants of adaptation determined as shown in *C*. Sample size discrepancies between *A* and *C* result from the fact that some cells showed a significant adaptation but their firing rate decay could not be fit satisfactorily. *C*: example of peristimulus time histograms (PSTHs) calculated for each contrast and contrast condition in a single cell. This cell showed significant adaptation during the high and medium constant-contrast stimulations. The firing rate decay was fit with an exponential (dark line) for these 2 conditions. *D*: population PSTH (all cells included) constructed after normalization of the response to the highest firing rate across conditions. The maximal value differs from unity because individual cells may not have reached their maximal firing rate with the high contrast and/or during the first second of the response. Thick black line, exponential fit to the population average for constant high and medium contrasts.

drifting grating (several seconds on average; Albrecht et al. 1984; McLean and Palmer 1996; Ohzawa et al. 1985; Sanchez-Vives et al. 2000; Sclar et al. 1989), but this is comparable to the values obtained with flashing stimuli (Fournier et al. 2011; Müller et al. 1999; Nelson 1991; Nowak and Barone 2009). Similar values of adaptation time constant were obtained when the analysis was performed on a population average of the PSTHs (Fig. 1*D*): 1.44 s for the high contrast and 1.22 s for the medium contrast.

Adaptation was considered to have reached a steady state at a time corresponding to 3τ. The static RF analysis in the constant-contrast conditions was restricted to this steady-state period. As adaptation time constant could depend on contrast, the longest τ value was used for the analysis period restriction. There was no restriction for cells that did not display significant contrast adaptation. The first 6 s of each block were excluded from analysis in cells that displayed a significant adaptation but for which the exponential fit returned an $r^2 < 0.6$.

Static receptive field analysis. The static RF features quantitatively analyzed in the present study were the amplitude and width of the RF, the subregion width, and the bright-dark subregion overlap. First, PSTHs (Fig. 2*B*) were computed for each bar polarity, contrast, and position between −100 and +250 ms relative to the bar presentation onset. The bin width was 10 ms. The data were interpolated at 1-ms resolution with a cubic spline. This interpolation was applied in the time dimension only, and therefore did not affect the data in the spatial dimension. Only the responses associated with stimulus appearance ("on" responses) were quantitatively analyzed in this study. Responses associated with stimulus withdrawal ("off" responses) were not examined. The data were also represented as space-time maps (DeAngelis et al. 1993a; McLean and Palmer 1989), which allow the decomposition of the response as functions of both space (*x*-axis) and time (*y*-axis); the response strength (*z*-axis) is represented by gray levels (Fig. 2*C*, Fig. 6*B*).

For determining response significance, we calculated the baseline variance across bar positions between −100 and 0 ms. A bright or dark bar subregion was considered significant if the response variance was larger than the mean baseline variance + 3 SD.

Three groups of cells were distinguished. The first corresponds to cells that displayed only one significant subregion, to either the dark or bright bar stimuli (Fig. 2), as reported in previous primate V1 studies (Bullier and Henry 1980; Conway and Livingstone 2003; Kagan et al. 2003; Schiller et al. 1976; Williams and Shapley 2007). This group corresponds to the "monocontrast" cells (Kagan et al. 2003). In monocontrast cells, the width and amplitude of the RF were directly obtained by fitting a Gaussian function[2] to the single significant subregion. The subregion profile (response amplitude R as a function of space x) was taken at the time of maximal variance in the maps (dotted lines in Fig. 2*C*). The Gaussian function was

$$R = R_{SA} + R_{\max}\exp\left[\frac{-(x - x_c)^2}{2\sigma^2}\right]$$

where R_{SA} corresponds to the spontaneous firing rate (in sp/s), R_{max} to the maximal amplitude of the response (in sp/s), x_c to the center of the subregion (in °), and σ to the standard deviation (in °). The width

[2] Our fitting procedure based on Gaussians assumes that the spatial distribution of input sources on a cortical cell resembles a Gaussian distribution, an assumption that is supported by anatomical studies (Buzás et al. 2006; Kennedy et al. 1994; Salin et al. 1989).

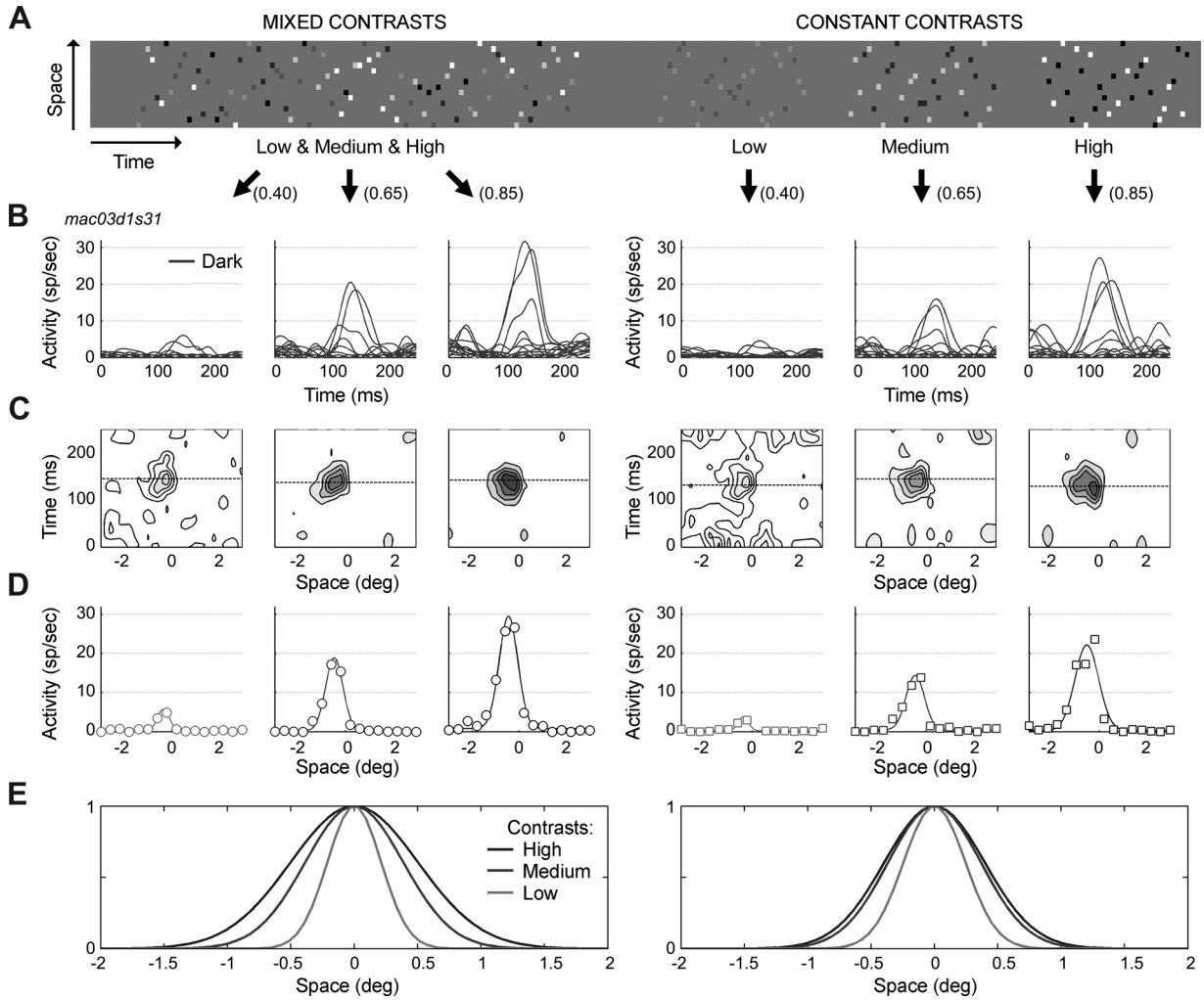

Fig. 2. Protocol and example. *A*: scheme of the receptive field (RF) mapping protocol. RFs were mapped with an optimally oriented bar that was flashed for 50 or 100 ms in 16 randomly chosen positions. The squares represent the bar position and its luminance as a function of time. The contrasts are labeled "low", "medium," and "high," and the actual values used for this cell are indicated on *right* of the arrows pointing toward the PSTHs (*B*). In the mixed-contrast block (*left*), the luminance (contrast) of the bar varied randomly from one presentation to the next. In the 3 constant-contrast blocks (*right*), the contrast was maintained constant for the whole duration of a block to low, medium, or high values, so that neurons had enough time to adapt to the contrast used for mapping the RF. *B*: PSTHs for each contrast and for each adaptation state. As this monocontrast cell showed no significant response to the bright bar, only the dark bar responses are shown. Each panel shows the spiking response for each position of the dark bar. Panels from *left* to *right* display the response to the low-, medium-, and high-contrast bars in the mixed-contrast condition (*left*) and in the constant-contrast condition (*right*). Increasing contrast evidently increased response amplitude. *C*: 3-dimensional representation of the spiking response amplitude (z-axis) as a function of both space (x-axis) and time (y-axis) (space-time maps). The isodensity lines represent increments of 20% in response amplitude, relative to the maximal response amplitude in each map. The horizontal dashed line in the maps indicates the time at which the response reached its peak (maximal variance). *D*: RF profile (response amplitude vs. space) taken at the time of maximal firing (dashed line in *C*). Circles (*left*) or squares (*right*) represent experimental data, and the continuous lines correspond to the Gaussian fitted to the data. *E*: Gaussian curves in *D* have been centered and normalized to the same height. Curves for low, medium, and high contrast are shown in the same plots (*left*: mixed contrast; *right*: constant contrast). The width taken at 5% of the maximal amplitude of the Gaussian was 2.45°, 1.91°, and 1.03° for the high, medium, and low contrasts, respectively, in the mixed-contrast condition and 1.91°, 1.76°, and 1.18° in the constant-contrast condition.

of the subregion was taken at 5% of the maximal amplitude and was calculated as $w_{5\%} = 4.896 \times \sigma$.

The second and third groups correspond to simple and complex cells. Both displayed significant "on" responses to both bright and bark bars. The subregion associated with the largest response variance across bar positions was designed as the "dominant" (dom) subregion, and the second subregion was termed "secondary" (sec). Both subregions were fitted with Gaussian functions. The time at which the secondary subregion profile was taken was constrained relative to that of the dominant subregion and corresponded to the time at which the variance was the highest, within ±5 ms, relative to the maximal variance of the dominant subregion.

We then computed the subregion overlap, using the overlap index (OI) of Schiller et al. (1976), modified to take the difference of subregion response amplitudes into account (Nowak et al. 2010). In a first step, the width of the secondary subregion was recalculated (w_{re}), such that it was taken at a height corresponding to 5% of the maximal amplitude in the dominant subregion:

$$w_{re} = 2 \times \left[-2\ln\left(\frac{0.05}{A_{\max(\sec)}/A_{\max(dom)}} \right) \right]^{0.5} \times \sigma_{\sec}$$

The overlap index was then calculated as

$$OI = \frac{0.5 \times \left(w_{5\%(dom)} + w_{re} \right) - \left| x_{c(dom)} - x_{c(\sec)} \right|}{0.5 \times \left(w_{5\%(dom)} + w_{re} \right) + \left| x_{c(dom)} - x_{c(\sec)} \right|}$$

Cells were considered as simple when the OI was <0.5 and complex otherwise.

In complex cells, we calculated the full RF width by combining the two subregions (w_C), as

$$w_C = 0.5 \times \left(w_{5\%(dom)} + w_{re}\right) + \left|x_{c(dom)} - x_{c(sec)}\right|$$

with w_{re} as defined above. The full RF width of complex cells corresponds to w_C provided $w_C > w_{5\%(dom)}$ and $w_C > w_{re}$. When this was not verified, that is, when one of the two subregions was larger and completely included the other, then the full RF width corresponded to that of this subregion. The amplitude of the complex RF was taken as the R_{max} of the dominant subregion.

Simple cells may possess more than two subregions in their RFs. To include these putative additional subregions in the RF width calculation, the dark bar response map was subtracted from the bright bar response map, and the difference response profile at the time of maximal variance was fitted with a Gabor function (Field and Tolhurst 1986; Jones and Palmer 1987b):

$$R = R_{SA} + R_{max}\exp\left[\frac{-(x - x_c)^2}{2\sigma^2}\right] \times \cos\left[\left\{2\pi F_{opt}(x - x_c)\right\} + \varphi\right]$$

R_{max}, x_c, and σ correspond to the Gaussian envelope of the Gabor, F_{opt} is the frequency of the RF (in cycles/°), and φ is its phase (in rad). The amplitude of the simple cell RF is R_{max}, and the width of the RF corresponds to the width of the Gaussian envelope taken at 5% of R_{max} ($w_{5\%}$).

Data were considered for further analysis only when the r^2 of fit was >0.7. This criterion was reached in 97% of the cases with a significant response. Median r^2 were 0.79, 0.84, and 0.90 for the low, medium, and high contrasts in the mixed-contrast condition and 0.86, 0.89, and 0.92 for the low, medium, and high contrasts in the constant-contrast condition (medians calculated from r^2 for Gabor fits in simple cell and single Gauss fits in monocontrast cells and mean r^2 of the pair of Gaussian fits in complex cells).

Area summation experiments. The mean firing rate was calculated for each stimulus diameter and contrast. For each contrast, the data were fitted to a difference of Gaussian integrals (Sceniak et al. 1999):

$$R = R_{SA} + K_e\int_{-s/2}^{s/2} e^{-(2y/a)^2}dy - K_i\int_{-s/2}^{s/2} e^{-(2y/b)^2}dy.$$

R_{SA} represents the spontaneous activity level, a the excitatory and b the inhibitory space constants, and K_e and K_i the excitatory and inhibitory gains, respectively. The fit parameters were used to derive the value of the preferred grating diameter, corresponding to the peak of the fit to the size tuning data (see Fig. 6*A*). Data for which the r^2 of fit was <0.7 were not considered for further analysis.

Statistics. Unless otherwise stated, the statistical significance of differences between paired groups was determined at the population level by the nonparametric Wilcoxon rank test. Sample size (n) given with statistics results does not correspond to a number of cells but to the number of pairs of cells for which a given comparison was carried out. Correlations were tested with the nonparametric Spearman rank correlation test.

RESULTS

Protocol and Examples

The present study is based on extracellular recordings that have been performed in areas V1 and V2 of three macaque monkeys. The sample consisted of 87 cells that responded to at least one of the six contrast conditions of our RF mapping protocol. Table 1 gives the sample size for each contrast and each stimulation protocol. Recordings were obtained both in the opercular and in the calcarine region of V1, such that RF eccentricity spanned ≈1° up to 16°. Seven cells were recorded in V2. As the effect of contrast on their RFs did not differ from that observed in V1, the corresponding data have been pooled with those of the V1 RFs.

The stimulation protocol was designed to examine the effect of contrast and contrast adaptation on the amplitude and width of the static RF revealed by the mapping procedure and on the overlap of the RF subregions (Fig. 2*A*). The mapping procedure consisted in flashing optimally oriented static bright and dark bars in 16 adjacent positions and with 3 different contrast values, referred to as "low," "medium," and "high" (see METHODS).

In a first block of stimulation, the contrast varied randomly from one bar presentation to the next. This corresponds to the "mixed-contrast" condition (Fig. 2*A*, *left*). In this condition, the contrast changed faster than the time required for contrast adaptation to take place. If adaptation occurred, it would have been for a contrast corresponding to the mean of the three contrasts in use. In this situation, the average contrast to which the neuron was adapted did not match with the contrast presented at a particular time. It was then possible to examine to effect of the contrast proper on the static RF features, independently of the effect of contrast adaptation.

In the second, third, and fourth stimulation blocks, the contrast was fixed to one value at a time for each block: low, medium, or high. These conditions are referred to as "constant-contrast" conditions (Fig. 2*A*, *right*). The effects of contrast adaptation on the static RF features were included in this situation, because each block of constant contrast lasted 16–30 s, in excess of the time required to achieve an adapted firing rate (see METHODS). It was then possible to examine the effect of contrast, including the effect of contrast adaptation, on the static RFs.

Table 1. *Sample and receptive field categories as a function of contrast and contrast presentation protocol*

	Mixed Contrast			Constant Contrast		
	Low	Medium	High	Low	Medium	High
RFs:						
Simple	2 (10%)	3 (5.7%)	7 (8.4%)	3 (10.7%)	4 (7.1%)	6 (6.9%)
Complex	8 (40%)	26 (49.1%)	46 (55.4%)	14 (50%)	30 (53.6%)	44 (50.6%)
Monocontrast	7 (35%)	19 (35.8%)	24 (28.9%)	6 (21.4%)	20 (35.7%)	30 (34.5%)
NC	3 (15%)	5 (9.4%)	6 (7.2%)	5 (17.9%)	2 (3.6%)	7 (8.0%)
Total	20	53	83	28	56	87

Numbers correspond to the number of cells with a significant response in at least 1 of the 6 conditions (3 contrasts × 2 stimulation protocols), grouped in 4 categories: 3 receptive field (RF) categories (see METHODS) and 1 for the nonclassified (NC) cells. Cells in the NC category displayed a significant secondary subregion, like simple and complex cells, but the r^2 of the Gaussian fit to this secondary subregion was <0.7, such that the fit parameters were not taken into account and the overlap index could not be calculated. Percentages are calculated for each contrast.

Results for a "monocontrast" cell are presented in Fig. 2, *B–E*. Figure 2*B* shows the PSTHs representing the response for each bar position and for each condition. This cell showed a strong response to the dark bar (traces in Fig. 2*B*) but no significant response to the bright bar (not shown). The response was monophasic, with no evidence of an "off" response. The maps shown in Fig. 2*C* summarize the dark bar response as a function of both space (*x*-axis) and time (*y*-axis). Response strength (*z*-axis) is indicated by gray levels, with an increase in darkening representing an increase in firing rate.

Examination of the PSTHs and the maps reveals decreased response amplitude when the contrast is decreased, both without (Fig. 2, *left*) and with (Fig. 2, *right*) matched adaptation. The RF profiles in Fig. 2*D* represent the response as a function of space, taken at the time of maximal variance in the maps (dotted line in maps). Time points of maximal variance were calculated individually for each contrast level and each adaptation condition. Each RF profile has been fitted with a Gaussian function. Decrease in response strength when contrast decreased is reflected by the decrease of the fitted Gaussian amplitude.

Not only the response amplitude but also the RF width decreased when contrast decreased. This is highlighted in Fig. 2*E*, where the Gaussian fits obtained for each contrast have been aligned to the same center and normalized to the same height. Decrease in width occurred both for the mixed-contrast (Fig. 2*E*, *left*) and constant-contrast (Fig. 2*E*, *right*) conditions. In this cell, however, the decrease in width was less marked when the cell was given enough time to adapt to the contrast of the stimuli (Fig. 2*E*, *right*). The effect of contrast on the width and amplitude of a complex RF is presented in Fig. 6, *B* and *C*.

RF Width Decreases When Contrast Decreases

We first examined, at the population level, the effect of contrast adaptation on RF width by comparing, for a given contrast, the RF width obtained in the mixed- and constant-contrast conditions (Table 2), but no significant effect of contrast adaptation was apparent, whatever the contrast considered (high contrast: $P = 0.2$; medium contrast: $P = 0.09$; low contrast: $P = 0.4$).

We then examined the effect of contrast proper on RF width. The results are summarized in Fig. 3 and Table 3. The scatterplots in Fig. 3, *A* and *D*, represent the width of the RF obtained with the medium contrast as a function of the width obtained at high contrast, whereas those in Fig. 3, *B* and *E*, show the width obtained with the low contrast as a function of that obtained at medium contrast. Data obtained in the mixed-contrast condition appear in Fig. 3, *A* and *B*, and those obtained in the constant-contrast conditions in Fig. 3, *D* and *E*. The diagonal in the scatterplots represents the equality line.

A large proportion of data points fall below the diagonal when the widths obtained at high and medium contrasts are compared (Fig. 3, *A* and *D*). This indicates a reduction of the RF width when the contrast is reduced from high to medium. This effect of contrast was very significant for both mixed ($P < 0.0001$, $n = 53$; Fig. 3*A*)- and constant ($P = 0.0007$, $n = 56$; Fig. 3*D*)-contrast conditions.

Width ratios for the different contrast comparisons are represented as box plots and cumulative histograms in Fig. 3, *C* and *F*, and Table 3. In the mixed-contrast condition, the median width ratio (medium/high; Fig. 3*C*) was 0.84 and in the constant- contrast condition (Fig. 3*F*) the median width ratio was 0.91. The 95% confidence intervals for the median (CI) are listed in Table 3.

The majority of data points also fall below the equality line when the widths obtained at low and medium contrasts are compared (Fig. 3, *B* and *E*), reflecting a decrease of the RF width when contrast was decreased from medium to low. At the population level, this effect was also significant (mixed-contrast condition: $P = 0.01$, $n = 20$; constant-contrast condition: $P = 0.002$, $n = 27$). In the mixed-contrast condition, the median width ratio (low/medium; Fig. 3*C*) was 0.77. In the constant-contrast condition, the median width ratio was 0.77, too (Fig. 3*F*).[3]

Reducing contrast significantly reduced RF width at the population level, and these changes were consistent across monkeys. However, heterogeneity is visible at the single-cell level (Fig. 3). We examined whether this heterogeneity could be ascribed to a different effect of contrast on RF width

[3] The effect of contrast on RF width was not significantly influenced by the sampling density of the RF. This was determined by examining whether changes in RF width with contrast depended on the number of bars that effectively entered in the RF. This number corresponds to the ratio RF width/bar width. For the medium contrast, the median was 6 bars/RF (range: 2–16). We compared the effects of contrast on RF width in 4 groups of cell pairs: those for which the RF was sampled by <4 bars at medium contrast ($n = 40$), those for which this number was 4–6 ($n = 43$), then 6–8.5 ($n = 36$), and those for which this number was >8.5 ($n = 37$). Mixed- and constant-contrast conditions were mixed in this analysis. We then tested whether the width ratios (low-to-medium or medium-to-high contrast ratios pooled) differed significantly between these groups, but we found no significant difference (ANOVA, $P = 0.9$). The median width ratios for the 4 groups were 0.81, 0.84, 0.82, and 0.92.

Table 2. *Effect of contrast adaptation on static RF features*

Parameters	Contrast		
	Low	Medium	High
RF amplitude ratio (constant/mixed)	1.06 [0.75–1.26]	1.10 [1.04–1.20]	0.88 [0.82–0.93]
	$P = 0.9$ ($n = 16$)	$P = 0.02$ ($n = 50$)	$P < 0.0001$ ($n = 83$)
RF width ratio (constant/mixed)	1.06 [0.89–1.21]	1.06 [0.98–1.13]	0.98 [0.94–1.01]
	$P = 0.4$ ($n = 16$)	$P = 0.09$ ($n = 50$)	$P = 0.2$ ($n = 83$)
Overlap index difference (constant − mixed)	0.00 [−0.05–0.25]	−0.03 [−0.08–0.04]	0.02 [0.01–0.06]
	$P = 0.6$ ($n = 10$)	$P = 0.9$ ($n = 28$)	$P = 0.03$ ($n = 50$)

Amplitude and width ratios are calculated from the value in the constant-contrast condition (matched adaptation) divided by the value in the mixed-contrast condition (non-matched adaptation). Overlap index (OI) difference is calculated as the value in the constant-contrast condition minus the value in the mixed-contrast condition. For each parameter comparison, the first line gives the median and the 95% confidence interval on the median in brackets. The second line gives the *P* value by paired Wilcoxon rank test, and *n* corresponds to the number of cell pairs for which the comparison has been carried out. The *n* is lower for the OI difference because the OI was calculated for cells that showed significant and well-fitted responses to both bright and dark bar stimuli.

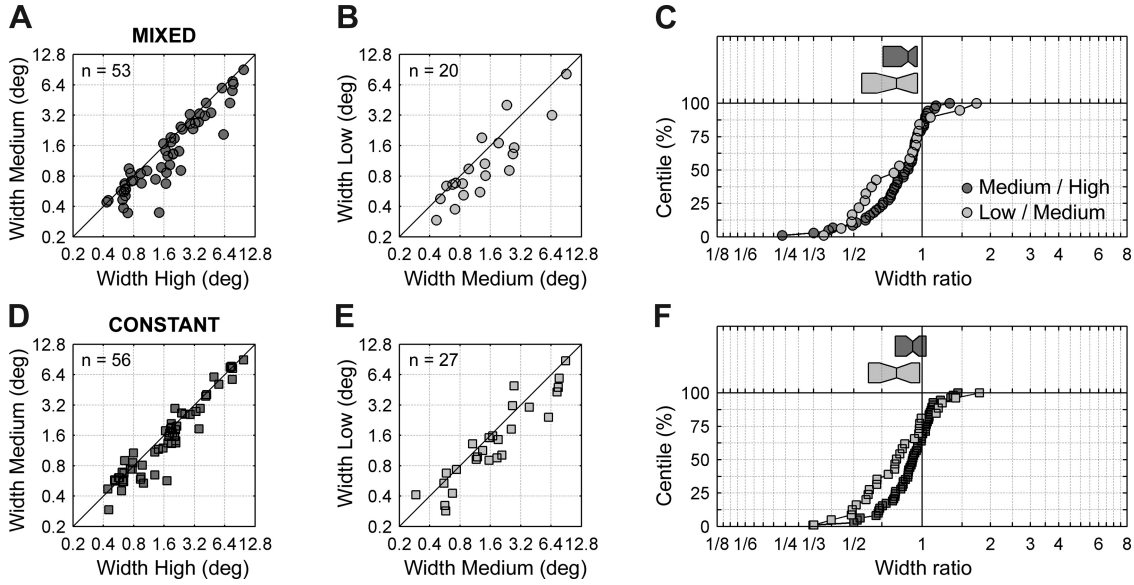

Fig. 3. RF width decreases when contrast decreases. Population data: mixed contrast condition (circles, *A–C*) and constant-contrast condition (squares, *D–F*). In *A* and *D* the width of the RF at medium contrast is represented as a function of the width obtained at high contrast, and in *B* and *E* the width of the RF at low contrast is represented as a function of the width obtained at medium contrast. *C* and *F*: cumulative distributions and box plots of width ratios: the RF width obtained at medium contrast has been divided by the width obtained at high contrast (dark gray), and the width obtained at low contrast has been divided by the width obtained at medium contrast (light gray). A value of 1 (unity line) would indicate that contrast had no effect on RF width. Both boxes and cumulative distributions appear shifted to left of the unity line, indicating a decrease of subregion width when contrast decreased. Box plot convention: the central vertical line indicates the median; the left and right borders of the box represent the 1st and 3rd quartiles, respectively; the intersections of the oblique lines starting at the median with the horizontal borders of the box correspond to the lower (*left*) and upper (*right*) 95% confidence interval of the median.

depending on where the neurons were recorded in the cortical layers. Recording sites have been localized for 63 neurons in V1 (see METHODS) and have been assigned to 4 groups of layers: infragranular layers ($n = 27$), layer 4C ($n = 5$), layer 4B ($n = 16$), and supragranular layers ($n = 15$). Width ratios, however, did not differ significantly between layers (Kruskal-Wallis test, $P = 0.8$).

Changes in RF width were sometimes accompanied by slight changes of the center position of the RF. We analyzed this issue by first calculating the difference in center position between two contrast conditions. These differences were then compared with the mean RF width obtained in the same conditions (not illustrated). Changes in center position were quite mild compared with the mean RF width: <10% of the mean width for ~80% of the cells and <20% for all the cells except for one cell in one contrast comparison.

Altogether these results indicate that the width of a cortical neuron RF decreases by 9–16% on average when contrast is decreased from high to medium and by an additional 23% when contrast is decreased from medium to low. When the width at low contrast is compared with the width at high contrast in the same cells (not illustrated), the width decrease was 51% in the mixed-contrast condition and 32% in the constant-contrast condition [width ratio 0.49, CI 0.42–0.78 ($n = 20$) and width ratio 0.68, CI 0.56–0.78 ($n = 28$)].

RF Amplitude Depends on Contrast and Contrast Adaptation

As expected, response amplitude depended strongly on stimulus contrast. This is summarized in Fig. 4 and Table 3. Most cells showed a decrease in response amplitude when the contrast was reduced from high to medium (Fig. 4, *A* and *D*) or

Table 3. *Effect of contrast on static RF features*

	Mixed Contrast		Constant Contrast	
	Low vs. medium	Medium vs. high	Low vs. medium	Medium vs. high
RF amplitude (ratio)	0.60 [0.49–0.70]	0.54 [0.44–0.62]	0.52 [0.38–0.59]	0.62 [0.50–0.72]
	$P = 0.0001$ ($n = 20$)	$P < 0.0001$ ($n = 53$)	$P < 0.0001$ ($n = 27$)	$P < 0.0001$ ($n = 56$)
RF width (ratio)	0.77 [0.56–0.94]	0.84 [0.76–0.91]	0.77 [0.63–0.97]	0.91 [0.84–0.97]
	$P = 0.01$ ($n = 20$)	$P < 0.0001$ ($n = 53$)	$P = 0.002$ ($n = 27$)	$P = 0.0007$ ($n = 56$)
Distance index	−0.20 [−0.65 to 0.09]	−0.52 [−0.96 to 0.25]	−0.24 [−0.99 to 0.20]	−0.58 [−1.01 to 0.35]
	$P = 0.2$ ($n = 20$)	$P < 0.0001$ ($n = 53$)	$P = 0.03$ ($n = 27$)	$P < 0.0001$ ($n = 56$)
Overlap index (difference)	−0.06 [−0.19 to 0.11]	−0.03 [−0.09 to 0.02]	−0.01 [−0.04 to 0.09]	−0.04 [−0.09 to 0.01]
	$P = 0.6$ ($n = 10$)	$P = 0.048$ ($n = 29$)	$P = 0.9$ ($n = 17$)	$P = 0.001$ ($n = 34$)

Amplitude and width ratios are calculated as low-to-medium and medium-to-high contrast ratios. Overlap index (OI) difference corresponds to the value at low contrast minus the value at medium contrast, or to the value at medium contrast minus the value at high contrast. For each parameter comparison, the first line gives the median, and the 95% confidence interval on the median in brackets. The second line gives the *P* value by paired Wilcoxon rank test, except for the distance index, where it corresponds to the *P* value of the median test; *n* corresponds to the number of cell pairs for which the comparison has been carried out. This number is lower for the OI difference because the OI calculation was restricted to cells that showed significant and well-fitted RF profiles for both bright and dark bars.

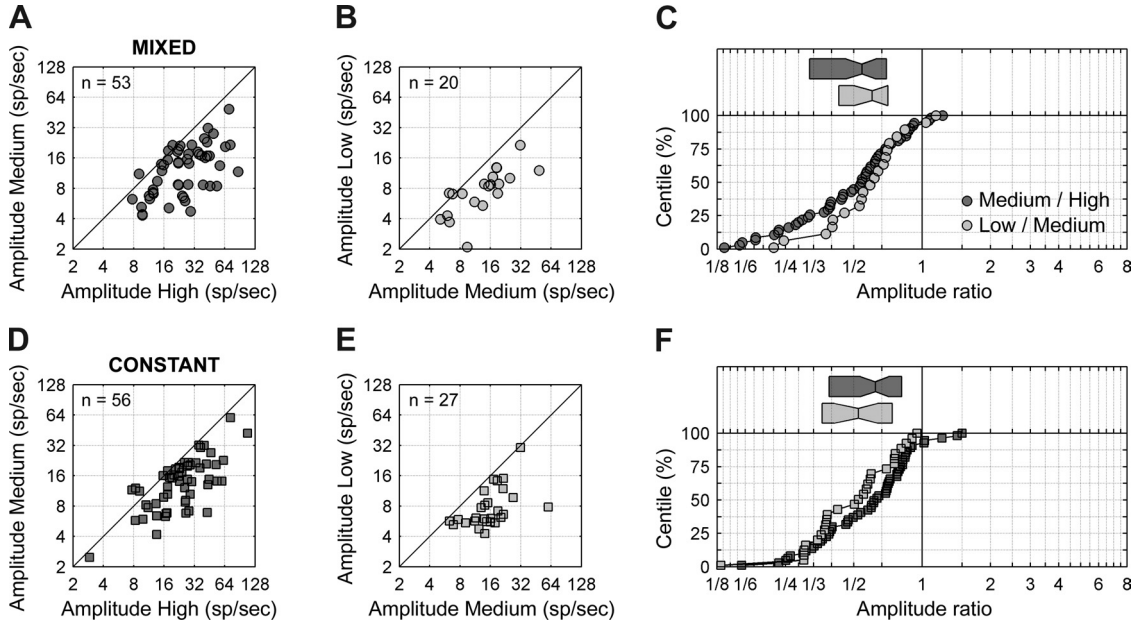

Fig. 4. RF amplitude decreases when contrast decreases. Same conventions as in Fig. 3. *A*, *C*, *D* and *F*: decreasing contrast from high to medium decreases response amplitude except in a couple of supersaturating cells. *B*, *C*, *E* and *F*: decreasing contrast from medium to low decreases response amplitude.

from medium to low (Fig. 4, *B* and *E*) ($P \leq 0.0001$ for the 4 comparisons).

In contrast to its lack of effect on RF width, contrast adaptation significantly modified response amplitude. The amplitude of the RF mapped with the high-contrast stimuli was significantly ($P < 0.0001$) lower in the constant-contrast condition compared with the mixed-contrast condition (Table 2). An opposite trend was observed with the medium contrast ($P = 0.02$, Table 2). There was no significant difference for the data obtained at low contrast ($P = 0.9$).

Closer to an Invariance of RF Width than to an Iceberg Effect

The results presented thus far indicate that both the width and the amplitude of the RF decreased when contrast decreased. One may argue that the effect of contrast on RF width is simply the consequence of an "iceberg effect," in which case the change in width should be proportional to the change in response amplitude. On the other hand, there are also a large number of cells for which the RF width did not appear to change much (data points on and near the diagonal in Fig. 3, *A–D*), even when their response amplitude was dramatically altered by contrast (see below). One may argue that such data imply that the RF width is contrast-invariant to a large extent. To determine whether the data were more consistent with an iceberg effect or with a contrast-invariant RF width, we compared the ratios of the widths obtained at two different contrasts with the values predicted from either an iceberg model or an invariance model.

The method we used is depicted with an example in Fig. 5*A*. The RF profiles obtained at medium and high contrast are presented with their fitted Gaussian curves. The Gaussian curves are replotted in Fig. 5*B*, but rearranged such that their tops are aligned. W_H corresponds to the width obtained at high contrast and W_L to the width obtained with the lowest contrast. W_L can be compared with the width predicted from the iceberg model, W_{IC}, which is the width taken from the Gaussian fitted to the high-contrast response, at the height corresponding to the amplitude of the low contrast RF profile, A_L (Fig. 5*B*). From visual inspection it is clear that, for this cell, the width predicted from the iceberg model, W_{IC}, is somewhat less than the one actually measured, W_L. This implies that the iceberg model overestimates the width decrease at low contrast in that particular case.

Mathematically, W_{IC} can be calculated using the sigma and amplitude of the Gaussian obtained at high contrast, σ_H and A_H, and the amplitude of the Gaussian obtained at low contrast, A_L, as

$$W_{IC} = \sigma_H \times 2 \times \sqrt{2 \times \log \frac{1}{1 - 0.95 \times (A_H/A_L)}}$$

If an iceberg effect was responsible for the change in width, then the width measured at low contrast should be identical to that predicted by the iceberg model, $W_L = W_{IC}$.

The invariance model, on the other hand, simply posits that the width obtained with the low contrast is equal to the width obtained with the high contrast, $W_L = W_H$. In the example of Fig. 5, *A* and *B*, $W_L < W_H$, implying that the RF width is not contrast-invariant either, strictly speaking.

Figure 5*C* compares the predictions of both models to the data actually obtained. Mixed- and constant-contrast conditions have been pooled. Each data point represents the amplitude ratio for two different contrasts as a function of the width ratio for the same contrasts. W_H/W_L and A_H/A_L refer here either to the high-to-medium contrast ratios or to the medium-to-low contrast ratios. The first noticeable result is that the width and amplitude ratios are not significantly correlated, in contrast to what would be expected from an iceberg model ($P = 0.16$ for high/medium contrast in the mixed condition and $P = 0.76$ in the constant-contrast condition; $P = 0.37$ for medium/low contrast in the mixed condition and $P = 0.51$ in the constant-contrast condition). Cells showing large changes in response

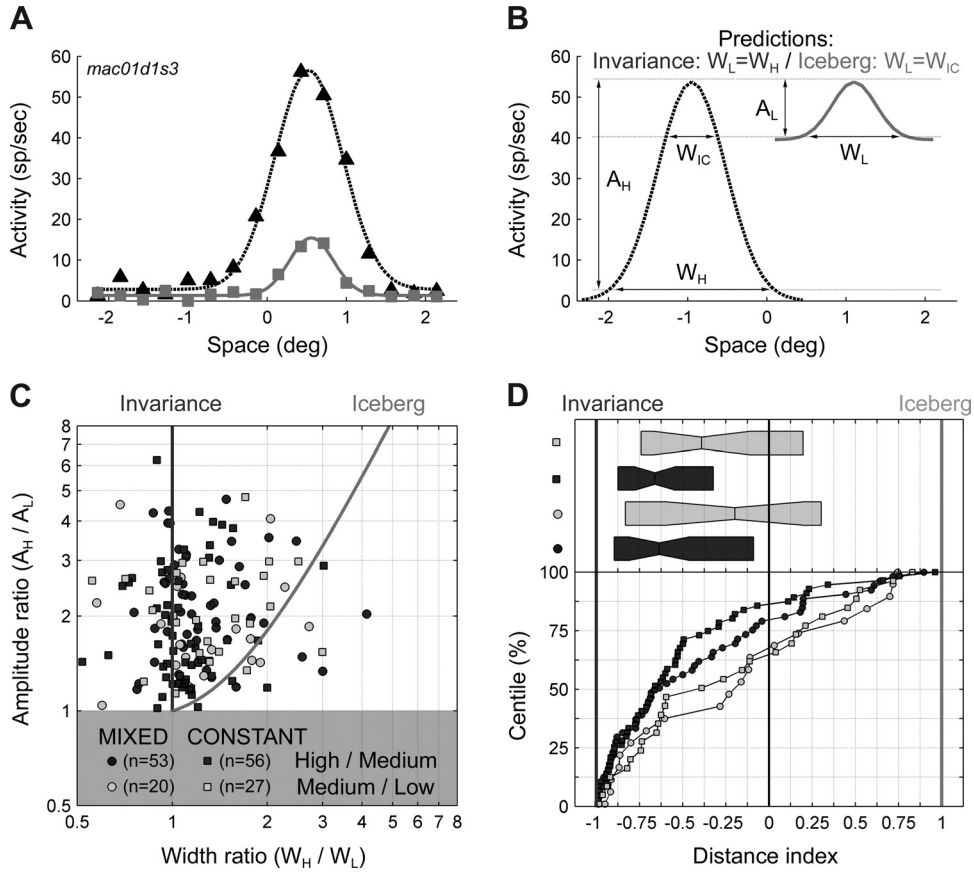

Fig. 5. Iceberg vs. invariance models. *A* and *B*: method and example. *A*: RF profiles of a monocontrast cell at medium (gray) and high (dark) contrast in constant-contrast condition. The symbols correspond to the experimental data and the lines to the Gaussian fitted to the data. *B*: the Gaussian fits have been redrawn such that their tops reach the same height. W_L is the width measured at the lowest contrast, and W_{IC} is the width expected from the iceberg model—when the tip of the Gaussian measured at high contrast "emerges" by a height corresponding to the amplitude of the Gaussian measured at low contrast (A_L). *C*: amplitude ratio (A_H/A_L) vs. width ratio (W_H/W_L), population data, and predictions for the iceberg (gray line) and invariance (black line) models. *D*: distribution of "distance index" as box plots and cumulative histograms.

amplitude may thus exhibit small changes in RF width, and the other way around.

The black vertical line labeled "invariance" in Fig. 5*C* corresponds to the prediction of the invariance model ($W_H/W_L = 1$ whatever A_H/A_L), while the gray line labeled "iceberg" represents the prediction for the iceberg model, calculated as A_H/A_L as a function of W_H/W_{IC}. It can be seen that the majority of data points fall between these two lines. In other words, the changes of RF width as a function of contrast are compatible neither with a pure iceberg model nor with a strict contrast invariance of the RF width.

To determine how far from each model the data fall on average, we reduced the width ratio shown in the scatterplot (Fig. 5*C*) to a distance index, DI, expressing the "distances" of each data point relative to the invariance and iceberg models.

$$DI = \frac{D_1 - D_2}{D_1 + D_2}$$

where D_1 is the distance between a data point and the invariance line along an axis parallel to the *x*-axis (width ratio) and D_2 the distance along the same axis to the iceberg model line. DI takes a value of -1 when the data conform to the invariance model and a value of $+1$ when the data conform to the iceberg model.

The distribution of DI values is presented in Fig. 5*D* (see also Table 3). For the mixed-contrast condition, the median DI values were -0.52 for the high vs. medium contrast comparison and -0.20 for the medium vs. low contrast comparison. For the constant-contrast conditions, the median DI values were -0.58 and -0.24 for the same contrast comparisons. A majority of value appears negative (Fig. 5*D*), and therefore closer to the invariance model. This trend is confirmed by a median test demonstrating that the median is significantly less than 0 for three of the four distributions (constant contrast: $P < 0.0001$ for high/medium, $P = 0.03$ for medium/low; mixed contrast: $P < 0.0001$ for high/medium but $P = 0.2$ for medium/low). The DI, therefore, are on average closer to the invariance model than to the iceberg model.

Comparing mixed- and constant-contrast conditions in Fig. 5*D* shows that DI did not depend on the adaptation state of the neurons ($P = 0.45$ for medium vs. high contrast DI and 0.44 for low vs. medium DI). This implies that adaptation did not lead to more invariance of the static RF width.

Altogether these results show that, although contrast significantly modifies RF width, the width changes do not genuinely depend on response strength and are overall closer to the expectation of a contrast-invariant RF width.

Effect of Contrast on Preferred Grating Diameter Is Opposite to That on Static RF Width

We have shown that the static RF width decreases when contrast decreases. This result is opposite to that obtained when the RF extent is deduced from size-tuning experiments. Indeed, numerous studies have shown that the apparent preferred stimulus diameter increases when the contrast is lowered (Cavanaugh et al. 2002; Kapadia et al. 1999; Sceniak et al. 1999; Sengpiel et al. 1997; Shushruth et al. 2009; Song and Li 2008; Tailby et al. 2007).

We therefore verified whether size-tuning experiments performed in our experimental conditions would provide results

that conform to those previously reported. Our results were indeed comparable to those of the previous studies in all respects. This is illustrated with one example in Fig. 6*A*. When stimulus diameter increased, the response first grew up to a peak beyond which the response amplitude decreased because of surround suppression. The peak response (arrowheads in Fig. 6*A*), as determined from the fitted function (see METHODS), was reached for a larger diameter when the contrast was lower. When flashing bars were used as stimuli in the same cell and with the same contrasts, it was found that reducing contrast reduced the width of the static RF instead (Fig. 6, *B* and *C*). Interestingly, the RF size estimates appeared quite similar at high contrast: the preferred stimulus diameter was 3.85°, and the width of the static RF was 3.90°. Discrepancies between the two RF size estimates therefore occurred at medium and low contrast: at medium contrast the values were 4.61° and 3.38°, respectively; at low contrast the divergence was even more pronounced (5.09° and 2.86°).

Size tuning was examined in a subsample of 29 cells. Figure 7*A* shows the preferred grating diameter at medium contrast compared with that at high contrast (Fig. 7*A*, *left*) and the preferred grating diameter at low contrast compared with that at medium contrast (Fig. 7*A*, *right*). Figure 7*B* presents the distribution of the ratios of preferred stimulus diameter for the different contrasts (medium/high and low/medium). At the population level, we also observed a significant increase of the preferred stimulus diameter when contrast decreased (medium vs. high: $P = 0.007$, median of the medium-to-high ratio 1.29, $n = 24$; low vs. medium: $P = 0.001$, median low-to-medium ratio = 1.27, $n = 18$).

Within this subsample of 29 cells, 26 cells also showed a significant response to the flashing bars for at least one contrast. The data presented in Fig. 7, *C* and *D*, correspond to those obtained in the constant-contrast condition. In this subsample, the RF width tended to decrease when contrast decreased. This decrease was significant for the medium vs. high contrast comparison ($P = 0.01$, $n = 17$) but not quite so for the low vs. medium comparison ($P = 0.08$), possibly as a result of the small number of pairs of data for this comparison ($n = 8$). The median of the medium-to-high RF width ratio was 0.84, and the median low-to-medium RF width ratio was 0.79 (Fig. 7*D*).

These experiments further allowed us to directly compare, in the same neurons, the width of the static RF and the preferred grating diameter at different contrasts (Fig. 8). Previous studies have shown that these two estimates of the RF size are roughly similar at high contrast (Cavanaugh et al. 2002; Kapadia et al. 1999; Levitt and Lund 2002; Song and Li 2008; Walker et al. 2000; Yao and Li 2002). However, comparisons have not been made, to our knowledge, for low-contrast stimuli. At high contrast, we also found that the preferred stimulus size, as determined from size-tuning experiments, is close to, although significantly ($P = 0.0005$) larger than, the width of the static RF (Fig. 8*B*): the preferred grating diameter represents 1.55 times the width of the static RF (CI 1.21–2.10, $n = 26$). However, the difference becomes much larger when contrast decreases. For the medium contrast, the ratio reaches a value of 2.64 (CI 2.02–3.40, $n = 20$; Fig. 8*B*) and the difference between the preferred grating diameter and the static RF width is largely significant ($P = 0.0004$). At low contrast, the ratio reaches an even larger value of 4.97 (CI 1.83–

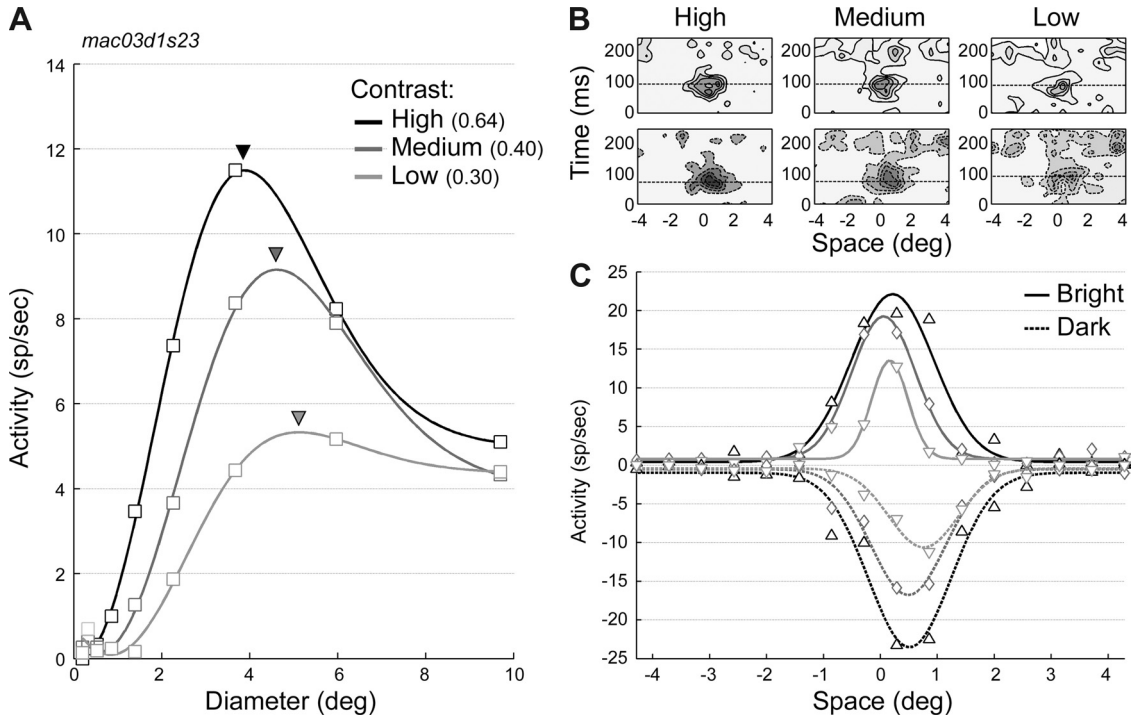

Fig. 6. Example of the opposite effect of contrast on preferred stimulus diameter, as determined from size-tuning measurements using drifting gratings, and static RF width, as determined with flashing bars. The same contrasts were used in the two protocols (64%, 40%, and 30%). *A*: response amplitude as a function of grating diameter. Squares represent experimental data, and continuous lines correspond to the difference of Gaussian integrals fitted to the data. Arrowheads indicate preferred stimulus diameter. Preferred grating diameter increased when contrast decreased. *B*: space-time map of the RF for the same cell. Bright bar responses are presented at *top* and dark bar responses at *bottom*. *C*: RF profiles taken at the time of maximal variance in the space-time maps (horizontal dashed lines in *B*). Symbols represent experimental data points, and lines correspond to the Gaussian fit to these data. Light, medium, and dark gray correspond to low, medium, and high contrast, respectively. Dark bar response and Gaussian fit scaled negatively for clarity. Static RF width decreased when contrast decreased.

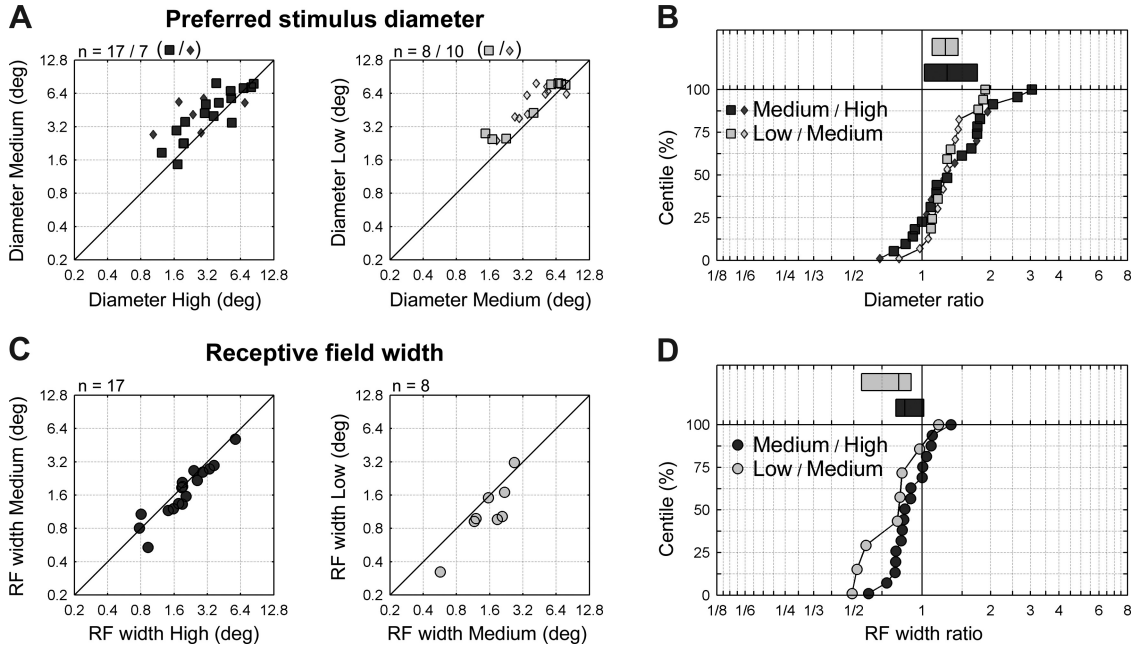

Fig. 7. Opposite effects of contrast on preferred grating diameter and static RF width: population data. Scatterplots in *A* represent the preferred grating size at medium contrast as a function of that obtained at high contrast (*left*) and at low contrast as a function of that obtained at medium contrast (*right*). The diagonals represent equality line. Squares correspond to the cells for which RF width has also been successfully estimated from bar mapping experiments. *B*: cumulative distribution and box plot summarizing the effect of contrast on preferred grating diameter. Preferred diameter ratios for low/medium (light gray) and medium/high (dark gray) contrasts appear shifted on the right of the unity line on average, indicating an increase in preferred grating diameter when contrast decreases. *C*: width of the static RF at medium contrast as a function of that obtained at high contrast (*left*) and at low contrast as a function of that at medium contrast (*right*). The sample is restricted to the cells for which size-tuning measurements have also been performed (*A*, *B*). This restricted sample shows the same trend as the whole sample (Fig. 3). *D*: cumulative distribution and box plot summarizing the effect of contrast on static RF width. Ratios for low/medium (light gray) and medium/high (dark gray) contrasts appear shifted on the left of the unity line on average, indicating a decrease of the static RF width when contrast decreases. Note opposite patterns in *B* and *D*.

7.70, $n = 10$; Fig. 8*B*) and the preferred grating diameter differs significantly from the static RF width ($P = 0.002$). In other words, at low contrast the static RF represents only ~20% of the preferred grating diameter, as a consequence of both a decrease in static RF width and an increase of preferred grating diameter when the contrast is decreased.

Another indication of a differential effect of contrast on preferred stimulus size and static RF extent appears when the correlations between the two measures are examined (Fig. 8*A*). At high contrast, preferred stimulus size and static RF extent were relatively well correlated ($\rho = 0.59$, $P = 0.002$). This correlation was less and only close to significance at medium contrast ($\rho = 0.42$, $P = 0.07$), and it was definitively lost at low contrast ($\rho = 0.16$, $P = 0.7$). This implies that the preferred grating diameter can be relatively well predicted from the static RF dimension at high contrast, but this predictive power seems to be lost at low contrast. These results suggest that different sets of connections are recruited by different stimuli and that this differential recruitment is gated by contrast (see DISCUSSION).

Contrast and Contrast Adaptation Weakly Affect RF Categorization

We classified the RFs in three different categories on the basis of the response to flashing light and dark bars: simple, complex, and monocontrast (see METHODS). Depending on con-

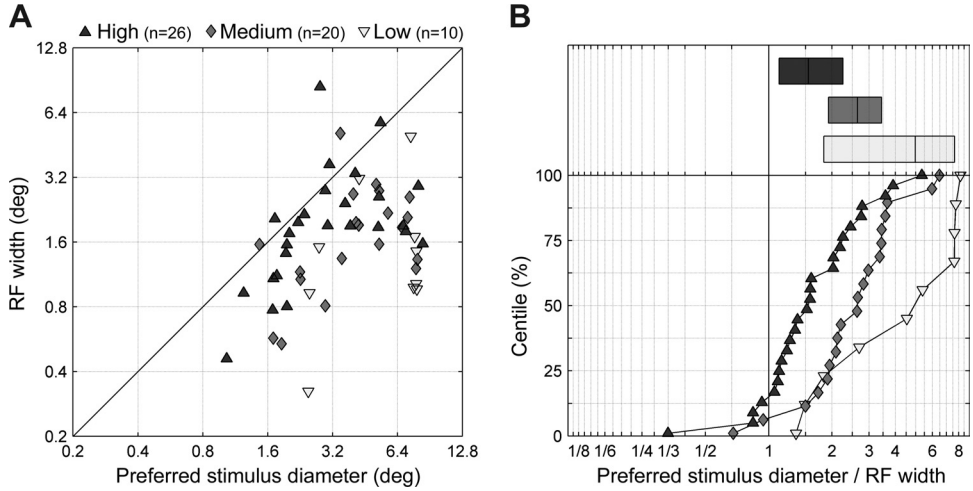

Fig. 8. Comparison of preferred grating diameter and static RF width measured in the same cells. *A*: scatterplot shows that the preferred grating diameter is larger than the static RF width. The difference is larger for lower contrasts. *B*: box plot and cumulative distribution of the ratio of preferred grating diameter to static RF width. For the population as a whole, the preferred grating diameter is larger than the static RF width, but the difference is much stronger at low contrast.

trast and adaptation state, monocontrast RFs represented between 21% and 36% of the RFs (Table 1). We first examined whether cells identified as monocontrast at low contrast were still monocontrast at a higher contrast, i.e., whether the absence of a significant secondary subregion was the consequence of a suboptimal activation of the cell at low contrast or whether monocontrast RFs genuinely correspond to a specific RF category, independently of stimulus intensity. Our results (not illustrated) provide support for the second possibility. In the constant-contrast condition, 4 of 5 (80%) monocontrast cells at low contrast remained monocontrast at medium contrast (the 5th cell became simple) and 15 of 20 (75%) monocontrast cells at medium contrast were still monocontrast at high contrast (among the 5 cells in which a significant secondary subregion appeared at high contrast, 4 were complex and 1 was simple).

In static RFs, simple and complex cells can be distinguished by the amount of subregion overlap (see, e.g., Heggelund 1986; Hubel and Wiesel 1962; Schiller et al. 1976). Subregion overlap was quantified with an overlap index (OI)[4] (see METHODS) that takes a value close to 0 when the subregions are well segregated (simple cells, example in Fig. 9*A*) and a value close to 1 when the subregions overlap substantially (complex cells, example in Fig. 9*B*). An OI value of 0.5 was used to separate simple and complex RFs.

As is typical of primate V1 (see, e.g., Conway and Livingstone 2003; Hubel and Wiesel 1968; Kagan et al. 2003), most RFs were complex (40–55%, depending on contrast and adaptation conditions; Table 1) whereas only 5–10% of the RFs were simple.

Decreasing contrast slightly decreased subregion overlap. This is summarized in Table 3 and in Fig. 9, *C* and *E*, which represent the difference of OI between two different contrasts (medium − high or low − medium). This decrease in overlap was moderate but significant when medium and high contrast were compared, both in mixed-contrast (median = −0.03, $P = 0.048$) and constant-contrast (median = −0.04, $P = 0.001$) conditions. Comparison between low and medium contrasts did not reveal significant changes in overlap ($P = 0.6$ and 0.9 for mixed- and constant-contrast conditions, respectively).

However, although contrast slightly modified the OI, in almost no case did we observe a cell that was complex to revert to simple when contrast was decreased, or the other way around. Assuming a simple/complex partitioning at an OI value of 0.5, it is easy to see that no cell switched categories for high vs. medium contrast in either the mixed (Fig. 9*D*)- or constant (Fig. 9*F*)-contrast condition. For low vs. medium contrast, 1 cell out of 10 in the mixed-contrast condition (Fig. 9*D*) and 1 out of 17 in the constant-contrast condition (Fig. 9*F*) switched categories, in both cases from complex at medium contrast to simple at low contrast.

Finally, we examined whether contrast adaptation affected simple/complex cell classification when this classification is derived from the OI calculated from the spatial profile of the static RF. At the population level, high-contrast adaptation resulted in a moderate decrease of subregion overlap ($P = 0.03$; Table 2). On the other hand, constant-contrast conditions did not significantly modify the OI for RFs mapped at medium ($P = 0.9$) and low ($P = 0.6$) contrasts compared with the mixed-contrast condition (Table 2). The simple/complex cell partitioning also remained essentially unaffected when matched and nonmatched adaptation were compared: category shifts occurred for 2 of 10 cells at low contrast, for 1 of 50 cells at high contrast, and for no cell at medium contrast (Fig. 9, *G–I*).

These data show that the partitioning between simple and complex cells, when based on the static RFs, remains quite robust with respect to changes in contrast and adaptation state. This is in contrast to the results obtained with drifting gratings (Crowder et al. 2007). The most likely explanation for this discrepancy is that RF generation and modulation depend on different sets of connections whose activation in turn depends on the features of the stimuli (see DISCUSSION).

DISCUSSION

Shrinkage of Static RF at Low Contrast

The first result of this study is that the width of the static RF, as revealed with a sparse noise stimulation protocol, decreases when contrast decreases. The median decrease amounts to 9% or 16% when contrast decreases from high to medium with or without matched adaptation, ~23% from medium to low, and 32% or 51% comparing high and low contrasts (Fig. 3).

The changes in RF width we obtained are incompletely explained by those observed in the retina. One study that can be directly compared to ours is that of Lee et al. (1985), who used flashing edges to probe the spatial resolution of retinal ganglion cells in the macaque as a function of contrast. They observed an enlargement of the center diameter of magnocellular-projecting ganglion cells at low contrast, a result opposite to ours; however, the center diameter of parvocellular-projecting cells showed a decreased diameter when contrast decreased.

At first sight, our results could have been explained by a synaptic RF whose amplitude is scaled by contrast, combined with a hard threshold and a linear input-output relationship. However, our analysis (Fig. 5) shows that the decrease in RF width is less than that expected from such an iceberg effect. Instead, changes in RF width appear to be closer to an invariance model than to an iceberg model. Mechanisms proposed to explain contrast invariance of orientation tuning may also apply here, that is, the presence of synaptic noise that leads to an expansive input-output relationship (see, e.g., Finn et al. 2007; Hansel and van Vreeswijk 2002; Miller and Troyer 2002; Persi et al. 2011). Yet these mechanisms may not be fully operative when high-frequency flashing stimuli are used, so as to lead to a completely contrast-invariant RF width (see also Nowak and Barone 2009 for contrast invariance of orientation tuning). Departure from invariance may have two explanations: in the first explanation, the subthreshold RF displays a width that is invariant with contrast but whose amplitude decreases when contrast decreases: a "true" iceberg effect would apply in this case. Alternatively, the subthreshold RF width may also decrease when contrast decreases, in which case the spiking RF would decrease as well, independently of the presence or absence of an expansive nonlinearity. Intracellular recording would be required to determine which mecha-

[4] Cells for which the bar orientation (chosen online according to the multiunit orientation tuning curve) differed by >30° from that preferred by the cell (calculated off-line after single-unit isolation) were excluded from this analysis.

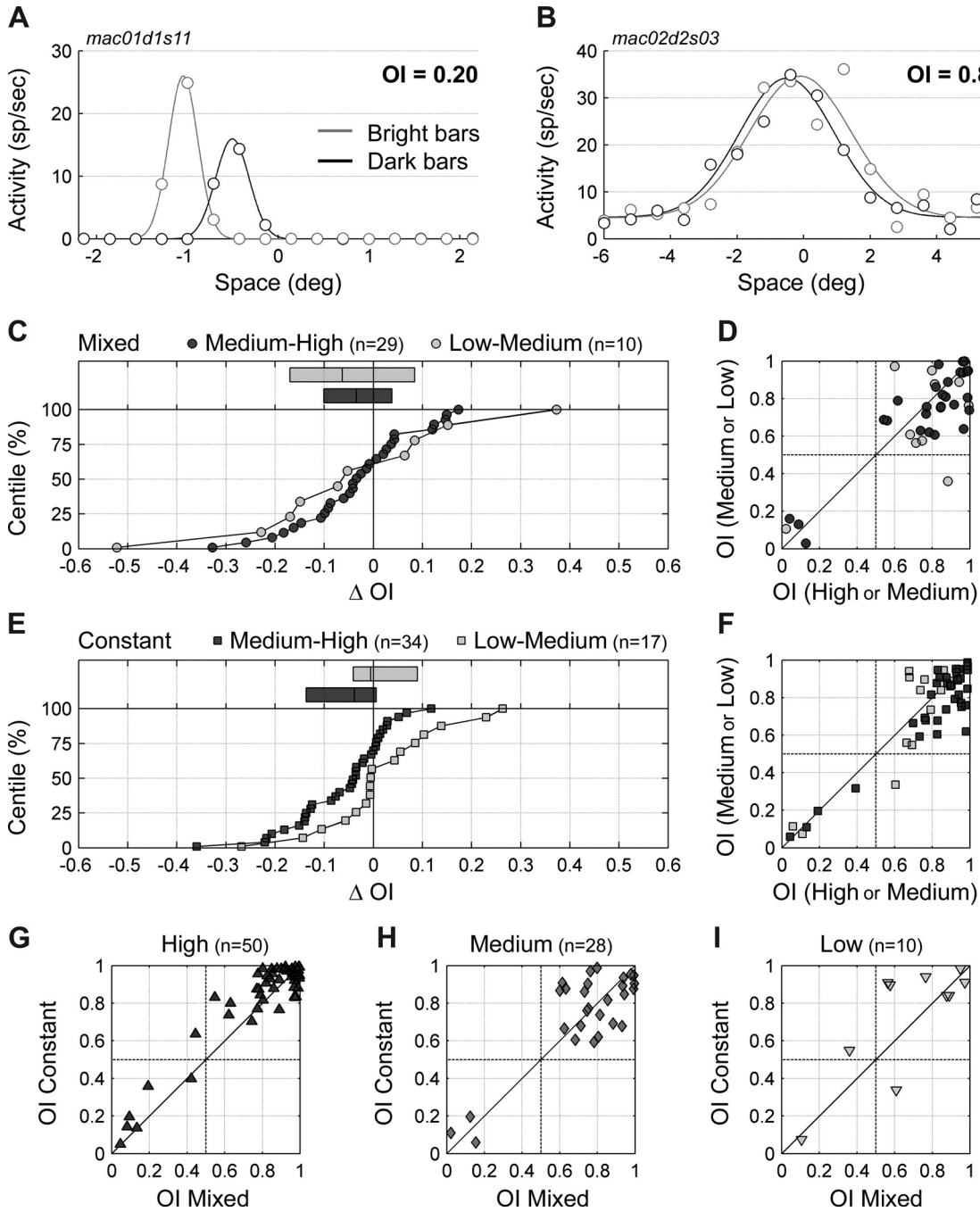

Fig. 9. *A*: subregion overlap in a simple cell. Light gray, subregion profiles for bright bar responses; black, subregion profiles for dark bar responses. Circles, experimental data; continuous lines, Gaussian fits. The 2 subregions overlap little [overlap index (OI) = 0.2], as is typical of simple cells. *B*: the subregion profiles for the bright and dark bar responses overlap almost completely in this second example (OI = 0.89), as is typical of complex cells. *C–F*: effect of contrast on subregion OI and on simple/complex cell distribution. *C* and *E*: cumulative distribution and box plot representation summarizing the changes in overlap induced by changes in contrast in the mixed (*C*)- and constant (*E*)-contrast conditions. The change in overlap is quantified as the difference of OI between 2 different contrasts (medium minus high in dark gray or low minus medium in light gray). *D*: OI at medium contrast compared with OI at high contrast (dark gray) and OI at low contrast compared with OI at medium contrast (light gray) in the mixed-contrast protocols. *F*: same as *D* but in the constant-contrast protocols. Horizontal and vertical dashed lines at OI = 0.5 mark the frontier between simple and complex cells. *G–I*: effect of contrast adaptation on subregion OI and on simple/complex cell distribution. OI is compared for the 2 adaptation conditions: nonmatched adaptation (mixed-contrast protocol, *x*-axis) and matched adaptation (constant-contrast protocol, *y*-axis).

nism is responsible (see Nowak et al. 2005 for the case of contrast adaptation).

Sceniak et al. (2002) examined the effect of contrast on spatial frequency tuning in macaque V1. They showed that reducing contrast does not change the preferred spatial frequency of cortical neurons but reduces the spatial frequency tuning bandwidth. In simple cells, spatial frequency tuning bandwidth depends on the number of subregions in the static RF (Andrews and Pollen 1979; DeAngelis et al. 1993b; Field and Tolhurst 1986; Movshon et al. 1978a). The results of

Sceniak et al. (2002) therefore predict that the optimal frequency of the static RF should not change when contrast decreases, whereas the number of subregions should increase. Unfortunately, our sample of simple cells was too small to perform relevant statistical comparisons, and the sparse noise stimulation technique we used does not allow the reconstruction of the subunits that constitute complex cell RFs. Furthermore, intracellular recording would be necessary to precisely assess the number of subthreshold subregions that also contribute to spatial frequency tuning (see Nowak et al. 2010). Consequently, we cannot state whether our results would lead to the same conclusion as those of Sceniak et al. (2002).

Relative Modulation and Subregion Overlap Show Different Contrast Sensitivity

Simple and complex RFs have traditionally been differentiated by the amount of subregion overlap revealed by flashing or drifting bars (Dean and Tolhurst 1983; Heggelund 1986; Hubel and Wiesel 1962; Mata and Ringach 2005; Schiller et al. 1976). An alternative metric to classify simple and complex cells is the "relative modulation" assessed with drifting gratings (e.g., Skottun et al. 1991). When examined with high-contrast stimuli the two methods provide reasonably similar classifications (Dean and Tolhurst 1983; Mata and Ringach 2005; Movshon et al. 1978a, 1978b). Recently, however, it has been shown that some of the cells that behave as complex cells with high contrast gratings display RM values typical of simple cells at low contrast (Crowder et al. 2007). Here we examined whether cells defined as complex by subregion overlap at high contrast showed a similar "simplification" at low contrast. Decreasing contrast significantly decreased subregion overlap (Fig. 9), thus indicating increased "simpleness" with decreased contrast. However, this decrease was relatively weak, and it was not sufficient to lead to RF category shifts, except for two cells (Fig. 9). The effect of contrast on RF classification therefore appears to depend on whether the stimuli are drifting gratings or flashing bars.

No Strong Effect of Contrast Adaptation on Static RF

In cat area 17, contrast adaptation can lead to a reduction of the amplitude of the static RF together with a moderate reduction of its width (Nowak et al. 2005). In the present study we have been able to replicate this effect on response amplitude but not on RF width (Table 2). However, here we used the mapping stimuli (flashing bars) to induce adaptation, and the relatively low energy of this stimulus may not have adapted the responses as strongly as the large drifting grating used to induce adaptation by Nowak et al. (2005). In addition, the Nowak et al. (2005) study was performed in cats, in which contrast adaptation may be more profound than in diurnal primates (see Allison et al. 1993; Sclar et al. 1989).

We recently showed that contrast invariance of orientation tuning is significantly improved by contrast adaptation (Nowak and Barone 2009). The static RF width, on the other hand, did not appear to be more invariant after adaptation (Fig. 5). If the same result applied to the RF length, then the implication would be that the (lack of) effect of contrast adaptation on the static RF does not predict the improvement of contrast invariance of orientation tuning by contrast adaptation.

As for the effect of contrast per se, we have not been able to demonstrate any strong effect of contrast adaptation on RF classification (Table 2, Fig. 9). In this respect, the results obtained with drifting gratings (Crowder et al. 2007) again are distinct from those presently obtained with flashing bars.

Opposite Effects of Contrast on RF Size Defined by Static Flashing Bars and Drifting Gratings

The results we obtained with flashing bars were opposite to those obtained with drifting gratings in size-tuning experiments, which consistently showed an increase in preferred grating diameter when contrast decreased (Cavanaugh et al. 2002; Kapadia et al. 1999; Sceniak et al. 1999; Sengpiel et al. 1997; Shushruth et al. 2009; Song and Li 2008; Tailby et al. 2007). We also performed size-tuning experiments in a subsample of cells, using the same contrasts as used for mapping the RFs. Our own results (Figs. 6 and 7) largely compare with those of these previous studies.

This further allowed us to directly compare (in the same neurons) the size of the RF with these two different methods. In accordance with previous studies (Cavanaugh et al. 2002; Kapadia et al. 1999; Levitt and Lund 2002; Song and Li 2008; Walker et al. 2000; Yao and Li 2002), the static RF and the preferred grating diameter were relatively similar at high contrast (Fig. 8) and the two measures of RF size were significantly correlated. The RF size estimate was nevertheless ~50% wider with drifting gratings. This could be explained by the presence of subthreshold regions that do not contribute to the static RF for the spiking response but may participate in the spiking response with gratings of appropriate dimension. The sample in the present study was dominated by complex cells, and, interestingly, it has been shown that in cat area 17 the subthreshold RF in complex cells is on average 60% wider than the spiking RF (Nowak et al. 2010).

At medium and low contrast, however, the two RF size estimates dramatically diverged. The static RF width decreased while the preferred grating diameter increased, and the two measurements were weakly (medium contrast) or not significantly (low contrast) correlated.

These comparisons indicate that the increase in preferred grating diameter at low contrast is not simply determined by contrast-dependent changes in the static RF extent. This rather suggests that the static RFs, as revealed by high-frequency flashing stimuli, and preferred stimulus size, as revealed by slowly drifting gratings, involve different sets of connections characterized by different gain mechanisms (see below). This also suggests that, in contrast to their preferred orientation, spatial frequency, and direction, neurons' preferred stimulus length, width, and area cannot be predicted directly from the static RF, especially at low and medium contrasts.

Connections and RF Generation

Our study reveals a number of discrepancies concerning the effect of contrast on RF extent and categorization, depending on whether the stimuli are slowly drifting gratings or high-frequency flashing bars: when contrast decreases the RF extent increases with the former but shrinks with the latter, and cells may change RF category with the former but less so with the latter. These discrepancies may reflect differences in terms of functional connectivity.

Indeed, the static RF revealed by high-contrast flashing bars in sparse noise protocols is quite likely to correspond to that generated by thalamocortical and short-range intracortical inputs (short range in the sense of connecting neurons with largely overlapping RFs). This is supported by extracellular recording studies (Alonso et al. 2001; Bullier et al. 1982; Tanaka et al. 1983) and anatomical tracing experiments (Angelucci and Sainsbury 2006; Salin et al. 1989). Calculations indicate that even the subthreshold static RF width in simple cells is comparable to that of the aggregate RF of afferent thalamic inputs (Nowak et al. 2010). This implies that long-range intracortical inputs do not contribute significantly to the subthreshold (Bringuier et al. 1999; Nowak et al. 2010) and suprathreshold RF revealed in sparse noise protocols. In this framework, decreasing contrast would decrease RF width simply by reducing input strength, although by an amount less than that expected from a simple iceberg effect (see above).

In contrast to high-frequency flashing bars, extended gratings can induce subthreshold responses away from the RF center. These responses are obtained over distances and with propagation speeds compatible with those expected from intrinsic horizontal connections (Benucci et al. 2007; Bringuier et al. 1999; Chavane et al. 2011; Girard et al. 2001; Grinvald et al. 1994). Horizontal connections also show an extent comparable to the low-contrast summation field observed in size-tuning experiments with gratings (Angelucci et al. 2002; Shushruth et al. 2009). When contrast increases, the apparent contribution of horizontal connections seems to be reduced (Nauhaus et al. 2009; but see Chavane et al. 2011), resulting in a reduction of the summation field diameter. Either this could be the result of a direct suppression of their participation when contrast increases, or their contribution may be masked by the recruitment of suppressive mechanisms. Whatever the underlying mechanism, this restores a high-contrast summation field whose dimension corresponds well with that of the high-contrast static RF.

Differential recruitment of intracortical connections may also explain the different effects of contrast and contrast adaptation on simple/complex cell classification, depending on whether the stimuli are high-frequency flashing bars or slowly drifting gratings. Intracortical connections apparently lack phase selectivity (DeAngelis et al. 1999). Grating stimuli therefore should induce an F0 component in the subthreshold response of cortical cells, including simple cells (Priebe et al. 2004). The F1 component may represent mostly the thalamocortical input to cortical cells, whereas the F0 component is likely to be mostly of intracortical origin, such that the contrast gain control of the two components is likely to be different (see, e.g., Sclar et al. 1990). Thus the contribution of the F1 component may be more prominent at low contrast, resulting in an increase of the relative modulation when contrast decreases (Crowder et al. 2007). On the other hand, bars flashed in a sparse noise protocol necessarily recruit less of the intracortical network, given their restricted spatial nature. Contrast gain control and contrast adaptation of the inputs may be less heterogeneous in these conditions, such that overlap index and related simple/complex cell classification may be less sensitive to contrast and contrast adaptation.

In short, the functional connectivity underlying the static RFs, as revealed by sparse flashing stimuli, may be dominated by thalamocortical and short-range intracortical connections, whereas the RFs revealed through size-tuning experiments with drifting gratings may be determined by thalamocortical inputs and short-range intracortical connections, and additionally by long-range intracortical connections and surround suppression. In this framework, center and/or surround mechanisms may be characterized by different gain and gain control mechanisms (Cavanaugh et al. 2002; Sceniak et al. 1999).

Our results show that contrast is one elemental feature of the stimuli, which profoundly affects the static RF features. This adds to the numerous studies that have shown that the spatiotemporal features of the static RF depend largely on the features of the stimuli that are used to reveal it (Bringuier et al. 1999; David et al. 2004; Fournier et al. 2011; Sharpee et al. 2008; Smyth et al. 2003; Victor et al. 2009; Williams and Shapley 2007; Yeh et al. 2009).

ACKNOWLEDGMENTS

We thank Andrew C. James for help with visual stimulation programs, Rosemarie Cano for help with electronics, Sebastien Aragones and Franck Lefèvre for animal care, Luc Renaud for histology, and Olivier Dufour for help with electrode track reconstruction. We also thank Douglas Mclelland for helpful comments on the manuscript.

GRANTS

This work was supported by the Centre National de la Recherche Scientifique, the Ministère délégué à la Recherche et aux Nouvelles Technologies (ACI Grant NIC 0085), and the Agence Nationale de la Recherche (ANR Grant 06-Neuro-025).

DISCLOSURES

No conflicts of interest, financial or otherwise, are declared by the author(s).

AUTHOR CONTRIBUTIONS

Author contributions: J.-B.D. analyzed data; J.-B.D. and L.G.N. interpreted results of experiments; J.-B.D. prepared figures; J.-B.D., P.G., P.B., and L.G.N. edited and revised manuscript; J.-B.D., P.G., P.B., and L.G.N. approved final version of manuscript; P.G., P.B., J.B., and L.G.N. performed experiments; L.G.N. conception and design of research; L.G.N. drafted manuscript.

REFERENCES

Abeles M. Quantification, smoothing, and confidence limits for single-units' histograms. *J Neurosci Methods* 5: 317–325, 1982.

Albrecht DG, Hamilton DB. Striate cortex of monkey and cat: contrast response function. *J Neurophysiol* 48: 217–237, 1982.

Albrecht DG, Farrar SB, Hamilton DB. Spatial contrast adaptation characteristics of neurones recorded in cat's visual cortex. *J Physiol* 347: 713–739, 1984.

Albrecht DG, Geisler WS. Motion selectivity and the contrast-response function of simple cells in the visual cortex. *Vis Neurosci* 7: 531–546, 1991.

Alitto HJ, Usrey WM. Influence of contrast on orientation and temporal frequency tuning in ferret primary visual cortex. *J Neurophysiol* 91: 2797–2808, 2004.

Allison JD, Casagrande VA, DeBruyn EJ, Bonds AB. Contrast adaptation in striate cortical neurons of the nocturnal bush baby (*Galago crassicaudatus*). *Vis Neurosci* 10: 1129–1139, 1993.

Alonso JM, Usrey WM, Reid RC. Rules of connectivity between geniculate cells and simple cells in cat primary visual cortex. *J Neurosci* 21: 4002–4015, 2001.

Anderson JS, Lampl I, Gillespie DC, Ferster D. The contribution of noise to contrast invariance of orientation tuning in cat visual cortex. *Science* 290: 1968–1972, 2000.

Andrews BW, Pollen DA. Relationship between spatial frequency selectivity and receptive field profile of simple cells. *J Physiol* 287: 163–176, 1979.

Angelucci A, Levitt JB, Walton EJS, Hupé JM, Bullier J, Lund JS. Circuits for local and global signal integration in primary visual cortex. *J Neurosci* 22: 8633–8646, 2002.

Angelucci A, Sainsbury K. Contribution of feedforward thalamic afferents and corticogeniculate feedback to the spatial summation area of macaque V1 and LGN. *J Comp Neurol* 498: 330–351, 2006.

Baker CL Jr, Cynader MS. Spatial receptive-field properties of direction-selective neurons in cat striate cortex. *J Neurophysiol* 55: 1136–1152, 1986.

Benucci A, Frazor RA, Carandini M. Standing waves and traveling waves distinguish two circuits in visual cortex. *Neuron* 55: 103–117, 2007.

Bringuier V, Chavane F, Glaeser L, Frégnac Y. Horizontal propagation of visual activity in the synaptic integration field of area 17 neurons. *Science* 283: 695–699, 1999.

Bullier J, Henry GH. Ordinal position and afferent input of neurons in monkey striate cortex. *J Comp Neurol* 193: 913–935, 1980.

Bullier J, Mustari MJ, Henry GH. Receptive-field transformations between LGN neurons and S-cells of cat striate cortex. *J Neurophysiol* 47: 417–438, 1982.

Buzás P, Kovacs K, Ferecsko AS, Budd JM, Eysel UT, Kisvarday ZF. Model-based analysis of excitatory lateral connections in the visual cortex. *J Comp Neurol 499*: 861–881, 2006.

Carandini M, Sengpiel F. Contrast invariance of functional maps in cat primary visual cortex. *J Vis* 4: 130–143, 2004.

Cardin JA, Palmer LA, Contreras D. Cellular mechanisms underlying stimulus-dependent gain modulation in primary visual cortex neurons in vivo. *Neuron* 59: 150–160, 2008.

Cavanaugh JR, Bair W, Movshon JA. Nature and interaction of signals from the receptive field center and surround in macaque V1 neurons. *J Neurophysiol* 88: 2530–2546, 2002.

Chavane F, Sharon D, Jancke D, Marre O, Frégnac Y, Grinvald A. Lateral spread of orientation selectivity in V1 is controlled by intracortical cooperativity. *Front Syst Neurosci* 5: 4, 2011.

Chen X, Han F, Poo MM, Dan Y. Excitatory and suppressive receptive field subunits in awake monkey primary visual cortex (V1). *Proc Natl Acad Sci USA* 104: 19120–19125, 2007.

Conway BR, Livingstone MS. Space-time maps and two-bar interactions of different classes of direction-selective cells in macaque V-1. *J Neurophysiol* 89: 2726–2742, 2003.

Crowder NA, van Kleef J, Dreher B, Ibbotson MR. Complex cells increase their phase sensitivity at low contrasts and following adaptation. *J Neurophysiol* 98: 1155–1166, 2007.

David SV, Vinje WE, Gallant JL. Natural stimulus statistics alter the receptive field structure of v1 neurons. *J Neurosci* 24: 6991–7006, 2004.

Dean AF, Tolhurst DJ. On the distinctness of simple and complex cells in the visual cortex of the cat. *J Physiol* 344: 305–325, 1983.

DeAngelis GC, Ohzawa I, Freeman RD. Spatiotemporal organization of simple-cell receptive fields in the cat's striate cortex. I. General characteristics and postnatal development. *J Neurophysiol* 69: 1091–1117, 1993a.

DeAngelis GC, Ohzawa I, Freeman RD. Spatiotemporal organization of simple-cell receptive fields in the cat's striate cortex. II. Linearity of temporal and spatial summation. *J Neurophysiol* 69: 1118–1135, 1993b.

DeAngelis GC, Ghose GM, Ohzawa I, Freeman RD. Functional micro-organization of primary visual cortex: receptive field analysis of nearby neurons. *J Neurosci* 19: 4046–4064, 1999.

Emerson RC, Citron MC, Vaughn WJ, Klein SA. Nonlinear directionally selective subunits in complex cells of cat striate cortex. *J Neurophysiol* 58: 33–65, 1987.

Fee MS, Mitra PP, Kleinfeld D. Automatic sorting of multiple unit neuronal signals in the presence of anisotropic and non-Gaussian variability. *J Neurosci Methods* 69: 175–188, 1996.

Field DJ, Tolhurst DJ. The structure and symmetry of simple-cell receptive field profiles in the cat's visual cortex. *Proc R Soc Lond B Biol Sci* 228: 379–400, 1986.

Finn IM, Priebe NJ, Ferster D. The emergence of contrast-invariant orientation tuning in simple cells of cat visual cortex. *Neuron* 54: 137–152, 2007.

Fournier J, Monier C, Pananceau M, Frégnac Y. Adaptation of the simple or complex nature of V1 receptive fields to visual statistics. *Nat Neurosci* 14: 1053–1060, 2011.

Gardner JL, Anzai A, Ohzawa I, Freeman RD. Linear and nonlinear contributions to orientation tuning of simple cells in the cat's striate cortex. *Vis Neurosci* 16: 1115–1121, 1999.

Girard P, Salin PA, Bullier J. Response selectivity of neurons in area MT of the macaque monkey during reversible inactivation of area V1. *J Neurophysiol* 67: 1437–1446, 1992.

Girard P, Hupé JM, Bullier J. Feedforward and feedback connections between areas V1 and V2 of the monkey have similar rapid conduction velocities. *J Neurophysiol* 85: 1328–1331, 2001.

Grinvald A, Lieke EE, Frostig RD, Hildesheim R. Cortical point-spread function and long-range lateral interactions revealed by real-time optical imaging of macaque monkey primary visual cortex. *J Neurosci* 14: 2545–2568, 1994.

Hansel D, van Vreeswijk C. How noise contributes to contrast invariance of orientation tuning in cat visual cortex. *J Neurosci* 22: 5118–5128, 2002.

Heggelund P. Receptive field organization of simple cells in cat striate cortex. *Exp Brain Res* 42: 89–98, 1981.

Heggelund P. Quantitative study of the discharge fields of single cells in cat striate cortex. *J Physiol* 373: 277–292, 1986.

Heggelund P, Moors J. Orientation selectivity and the spatial distribution of enhancement and suppression in receptive fields of cat striate cortex cells. *Exp Brain Res* 52: 235–247, 1983.

Hubel DH, Wiesel TN. Receptive fields, binocular interaction and functional architecture in the cat's visual cortex. *J Physiol* 160: 106–154, 1962.

Hubel DH, Wiesel TN. Receptive fields and functional architecture of monkey striate cortex. *J Physiol* 195: 215–243, 1968.

Jones JP, Palmer LA. The two-dimensional spatial structure of simple receptive fields in cat striate cortex. *J Neurophysiol* 58: 1187–1211, 1987a.

Jones JP, Palmer LA. An evaluation of the two-dimensional Gabor filter model of simple receptive fields in cat striate cortex. *J Neurophysiol* 58: 1233–1258, 1987b.

Kagan I, Gur M, Snodderly DM. Spatial organization of receptive fields of V1 neurons of alert monkeys: comparison with responses to gratings. *J Neurophysiol* 88: 2557–2574, 2003.

Kapadia MK, Westheimer G, Gilbert CD. Dynamics of spatial summation in primary visual cortex of alert monkeys. *Proc Natl Acad Sci USA* 96: 12073–12078, 1999.

Kennedy H, Salin P, Bullier J, Horsburgh G. Topography of developing thalamic and cortical pathways in the visual system of the cat. *J Comp Neurol* 348: 298–319, 1994.

Lampl I, Anderson JS, Gillespie DC, Ferster D. Prediction of orientation selectivity from receptive field architecture in simple cells of cat visual cortex. *Neuron* 30: 263–274, 2001.

Lee BB, Wehrhahn C, Westheimer G, Kremers J. The spatial precision of macaque ganglion cell responses in relation to vernier acuity of human observers. *Vision Res* 35: 2743–2758, 1995.

Levitt JB, Lund JS. The spatial extent over which neurons in macaque striate cortex pool visual signals. *Vis Neurosci* 19: 439–452, 2002.

Li CY, Creutzfeldt OD. The representation of contrast and other stimulus parameters by single neurons in area 17 of the cat. *Pflügers Arch* 401: 304–314, 1984.

Maffei L, Fiorentini A, Bisti S. Neural correlate of perceptual adaptation to gratings. *Science* 182: 1036–1038, 1973.

Mata ML, Ringach DL. Spatial overlap of ON and OFF subregions and its relation to response modulation ratio in macaque primary visual cortex. *J Neurophysiol* 93: 919–928, 2005.

McLean J, Palmer LA. Contribution of linear spatiotemporal receptive field structure to velocity selectivity of simple cells in area 17 of cat. *Vision Res* 29: 675–679, 1989.

McLean J, Palmer LA. Contrast adaptation and excitatory amino acid receptors in cat striate cortex. *Vis Neurosci* 13: 1069–1087, 1996.

Merill EG, Ainsworth A. Glass-coated platinum-plated tungsten microelectrodes. *Med Biol Eng* 10: 662–72, 1972.

Miller KD, Troyer TW. Neural noise can explain expansive, power-law nonlinearities in neural response functions. *J Neurophysiol* 87: 653–659, 2002.

Movshon JA, Thompson ID, Tolhurst DJ. Spatial summation in the receptive fields of simple cells in the cat's striate cortex. *J Physiol* 283: 53–77, 1978a.

Movshon JA, Thompson ID, Tolhurst DJ. Receptive field organization of complex cells in the cat's striate cortex. *J Physiol* 283: 79–99, 1978b.

Müller JR, Metha AB, Krauskopf J, Lennie P. Rapid adaptation in visual cortex to the structure of images. *Science* 285: 1405–1408, 1999.

Nauhaus I, Busse L, Carandini M, Ringach DL. Stimulus contrast modulates functional connectivity in visual cortex. *Nat Neurosci* 12: 70–76, 2009.

Nelson SB. Temporal interactions in the cat visual system. I. Orientation-selective suppression in the visual cortex. *J Neurosci* 11: 344–356, 1991.

Niell CM, Stryker MP. Highly selective receptive fields in mouse visual cortex. *J Neurosci* 28: 7520–7536, 2008.

Nowak LG, Munk MHJ, Girard P, Bullier J. Visual latencies in areas V1 and V2 of the macaque monkey. *Vis Neurosci* 12: 371–384, 1995.

Nowak LG, Sanchez-Vives MV, McCormick DA. Role of synaptic and intrinsic membrane properties in short-term receptive field dynamics in cat area 17. *J Neurosci* 25, 1866–1880, 2005.

Nowak LG, Barone P. Contrast adaptation contributes to contrast-invariance of orientation tuning of primate V1 cells. *PLoS One* 4: e4781, 2009.

Nowak LG, Sanchez-Vives MV, McCormick DA. Spatial and temporal features of synaptic to discharge receptive field transformation in cat area 17. *J Neurophysiol* 103: 677–697, 2010.

Ohzawa I, Sclar G, Freeman RD. Contrast gain control in cat's visual system. *J Neurophysiol* 54: 651–667, 1985.

Pack CC, Conway BR, Born RT, Livingstone MS. Spatiotemporal structure of nonlinear subunits in macaque visual cortex. *J Neurosci* 26: 893–907, 2006.

Palmer LA, Davis TL. Receptive-field structure in cat striate cortex. *J Neurophysiol* 46: 260–276, 1981.

Persi E, Hansel D, Nowak L, Barone P, van Vreeswijk C. Power-law input-output transfer functions explain the contrast-response and tuning properties of neurons in visual cortex. *PLoS Comput Biol* 7: e1001078, 2011.

Priebe NJ, Mechler F, Carandini M, Ferster D. The contribution of spike threshold to the dichotomy of cortical simple and complex cells. *Nat Neurosci* 7: 1113–1122, 2004.

Priebe NJ, Ferster D. Direction selectivity of excitation and inhibition in simple cells of the cat primary visual cortex. *Neuron* 45: 133–145, 2005.

Reid RC, Soodak RE, Shapley RM. Directional selectivity and spatiotemporal structure of receptive fields of simple cells in cat striate cortex. *J Neurophysiol* 66: 505–529, 1991.

Rust NC, Schwartz O, Movshon JA, Simoncelli EP. Spatiotemporal elements of macaque V1 receptive fields. *Neuron* 46: 945–956, 2005.

Salin PA, Bullier J, Kennedy H. Convergence and divergence in the afferent projections to cat area 17. *J Comp Neurol* 283: 486–512, 1989.

Sanchez-Vives MV, Nowak LG, McCormick DA. Membrane mechanisms underlying contrast adaptation in cat area 17 in vivo. *J Neurosci* 20, 4267–4285, 2000.

Sasaki KS, Ohzawa I. Internal spatial organization of receptive fields of complex cells in the early visual cortex. *J Neurophysiol* 98: 1194–1212, 2007.

Sceniak MP, Ringach DL, Hawken MJ, Shapley R. Contrast's effect on spatial summation by macaque V1 neurons. *Nat Neurosci* 2: 733–739, 1999.

Sceniak MP, Hawken MJ, Shapley R. Contrast-dependent changes in spatial frequency tuning of macaque V1 neurons: effects of a changing receptive field size. *J Neurophysiol* 88: 1363–1373, 2002.

Schiller PH, Finlay BL, Volman SF. Quantitative studies of single-cell properties in monkey striate cortex. I. Spatiotemporal organization of receptive fields. *J Neurophysiol* 39: 1288–1319, 1976.

Sclar G, Freeman RD. Orientation selectivity in the cat's striate cortex is invariant with stimulus contrast. *Exp Brain Res* 46: 457–461, 1982.

Sclar G, Lennie P, DePriest DD. Contrast adaptation in striate cortex of macaque. *Vision Res* 29: 747–755, 1989.

Sclar G, Maunsell JH, Lennie P. Coding of image contrast in central visual pathways of the macaque monkey. *Vision Res* 30: 1–10, 1990.

Sengpiel F, Sen A, Blakemore C. Characteristics of surround inhibition in cat area 17. *Exp Brain Res* 116: 216–228, 1997.

Sharpee TO, Miller KD, Stryker MP. On the importance of static nonlinearity in estimating spatiotemporal neural filters with natural stimuli. *J Neurophysiol* 99: 2496–2509, 2008.

Shushruth S, Ichida JM, Levitt JB, Angelucci A. Comparison of spatial summation properties of neurons in macaque V1 and V2. *J Neurophysiol* 102: 2069–2083, 2009.

Skottun BC, Bradley A, Sclar G, Ohzawa I, Freeman RD. The effects of contrast on visual orientation and spatial frequency discrimination: a comparison of single cells and behavior. *J Neurophysiol* 57: 773–786, 1987.

Skottun BC, De Valois RL, Grosof DH, Movshon JA, Albrecht DG, Bonds AB. Classifying simple and complex cells on the basis of response modulation. *Vision Res* 31: 1079–1086, 1991.

Smyth D, Willmore B, Baker GE, Thompson ID, Tolhurst DJ. The receptive-field organization of simple cells in primary visual cortex of ferrets under natural scene stimulation. *J Neurosci* 23: 4746–4759, 2003.

Song XM, Li CY. Contrast-dependent and contrast-independent spatial summation of primary visual cortical neurons of the cat. *Cereb Cortex* 18: 331–336, 2008.

Szulborski RG, Palmer LA. The two-dimensional spatial structure of nonlinear subunits in the receptive fields of complex cells. *Vision Res* 30: 249–254, 1990.

Tailby C, Solomon SG, Peirce JW, Metha AB. Two expressions of "surround suppression" in V1 that arise independent of cortical mechanisms of suppression. *Vis Neurosci* 24: 99–109, 2007.

Tanaka K. Cross-correlation analysis of geniculostriate neuronal relationship in cats. *J Neurophysiol* 49: 1303–1318, 1983.

Tolhurst DJ, Dean AF. The effects of contrast on the linearity of spatial summation of simple cells in the cat's striate cortex. *Exp Brain Res* 79: 582–588, 1990.

Touryan J, Felsen G, Dan Y. Spatial structure of complex cell receptive fields measured with natural images. *Neuron* 45: 781–791, 2005.

Usrey WM, Sceniak MP, Chapman B. Receptive fields and response properties of neurons in layer 4 of ferret visual cortex. *J Neurophysiol* 89: 1003–1015, 2003.

Van Hooser SD, Heimel JA, Chung S, Nelson SB, Toth LJ. Orientation selectivity without orientation maps in visual cortex of a highly visual mammal. *J Neurosci* 25: 19–28, 2005.

Victor JD, Mechler F, Ohiorhenuan I, Schmid AM, Purpura KP. Laminar and orientation-dependent characteristics of spatial nonlinearities: implications for the computational architecture of visual cortex. *J Neurophysiol* 102: 3414–3432, 2009.

Walker GA, Ohzawa I, Freeman RD. Suppression outside the classical cortical receptive field. *Vis Neurosci* 17: 369–379, 2000.

Williams PE, Shapley RM. A dynamic nonlinearity and spatial phase specificity in macaque V1 neurons. *J Neurosci* 27: 5706–5718, 2007.

Yao H, Li CY. Clustered organization of neurons with similar extra-receptive field properties in the primary visual cortex. *Neuron* 35: 547–553, 2002.

Yeh CI, Xing D, Williams PE, Shapley RM. Stimulus ensemble and cortical layer determine V1 spatial receptive fields. *Proc Natl Acad Sci USA* 106: 14652–14657, 2009.